

THE IMPACT OF MICROSTRUCTURE AND PHYSICAL PROPERTIES ON
PORE CLOSE-OFF AT WAIS DIVIDE AND MEGADUNES

A Thesis

Submitted to the Faculty

in partial fulfillment of the requirements for the

degree of

Master of Science

by

Stephanie Ann Gregory

Thayer School of Engineering

Dartmouth College

Hanover, New Hampshire

May 2013

Examining Committee:

Chairman _____
(Dr. Mary Albert)

Member _____
(Dr. Ian Baker)

Member _____
(Dr. Zoe Courville)

F. Jon Kull
Dean of Graduate Studies

Thayer School of Engineering
Dartmouth College

“The impact of microstructure and physical properties on
pore close-off at WAIS Divide and Megadunes”

Stephanie Ann Gregory

Master of Science

Dr. Mary Albert
Dr. Ian Baker
Dr. Zoe Courville

Abstract

The depth at which atmospheric air becomes entrapped into bubbles at the bottom of the firn column plays an important role in creating an appropriate age difference (Δ age) between the age of the gas and the age of the ice at a given depth within an ice core. The top 50-120m of an ice sheet consists of polar firn, a porous media, acting as a filter smoothing atmospheric signals as air rapidly diffuses to the base of the firn column on a decadal time scale. The density, permeability and microstructure of two firn cores from different local climates, WAIS Divide and Megadunes, were examined. The microstructure of the firn was determined to have a greater impact on permeability and pore close-off than density had.

Comparison between sites show that, at a given density, the pore structure of Megadunes firn was less complex and tortuous with greater permeability than WAIS Divide firn, characterized by smaller grains and a more complex pore structure. For both WAIS Divide and Megadunes, fine grained layers experience close-off shallower in the firn column than do coarse grained layers, regardless of which grain sized layer is the

more dense layer at depth. Pore close-off occurs at an open porosity that is accumulation rate dependent. Low accumulation sites, with coarser grains, close-off at lower open porosities (<10%) than the open porosity (>10%) of high accumulation sites with finer grains. The greater the variability between fine grained and coarse grain firn layers at depth, the longer the lock-in zone will be. At Megadunes, the fine grained layers are remnants of past accumulation sites on the ice sheet surface. These layers reach pore close-off significantly shallower than densification models predict for polar sites with similar local climate. A shallow LID would decrease Δ age to values similar to those predicted through $\delta^{15}\text{N}$ reconstructions of firn thickness. Application of this work in future studies could reduce the data-model mismatch, improve modeling of the lock-in zone through firn densification models, and reduce the need for inverse firn air modeling.

Acknowledgements

Table of Contents

Abstract	iv
Acknowledgements	vi
Table of Contents	vii
List of Tables	ix
List of Figures	x
1 Introduction	1
2 Background	4
2.1 <i>Pore Close-off</i>	4
2.1.1 The Lock-in Zone	4
2.1.2 Parameters Influencing Pore Close-off	5
2.1.3 Firn Densification Models and Pore Close-off	7
2.2 <i>Densification of Firn</i>	8
2.3 <i>Gas Transport in Porous Polar Firn</i>	11
2.3.1 Permeability and Diffusivity	11
2.3.2 Firn Air Measurements	14
2.3.3 Firn Air Models	16
2.4 <i>Data-model Mismatch</i>	18
2.5 <i>Microstructure of Polar Firn</i>	19
2.6 <i>Megadunes</i>	22
2.7 <i>Site Characteristics</i>	24
2.7.1 Megadunes	24
2.7.2 WAIS Divide	25
3 Methods	27
3.1 <i>Visual Stratigraphy</i>	27
3.2 <i>Bulk Density</i>	27
3.3 <i>Permeability</i>	28
3.3.1 Permeability of Firn Samples.....	28
3.3.2 Calibration of the Permeameter with Glass Beads.....	29
3.3.3 Wedged Membrane Testing for Megadunes Permeability.....	31
3.4 <i>Micro Computed Tomography</i>	32
3.4.1 Micro Computed Tomography Acquisition and Settings	32
3.4.2 Microstructural Properties	35
4 Results	40
4.1 <i>Stratigraphy</i>	40
4.2 <i>Density</i>	41
4.3 <i>Permeability</i>	44
4.4 <i>Microstructure</i>	47
4.4.1 Visual 3D Reconstructions	47

4.4.2 Microstructural Parameters	49
4.4.3 Porosity	53
5 Discussion	60
<i>5.1 Impact of Megadunes on Age</i>	<i>60</i>
5.1.1 Shallow LID due to Antidunes Presence	60
5.1.2 Antidunes and the data-model Mismatch	65
<i>5.2 Layering in Polar Firn</i>	<i>67</i>
<i>5.3 Impact of Physical Properties on Pore Close-off</i>	<i>70</i>
5.3.1 Macroscopic Properties: Density and Permeability	70
5.3.2 Application to Densification Models and LIZ Characteristics	71
5.3.3 Application to Firn Air Models.....	77
5.3.4 Summary of Local Climate Impacts on Pore Close-off and Gas Transport .	79
6 Conclusion	82
7 Future Work	86
8 References	87

List of Tables

Table 1: Summary of firn air sampling sites and characteristics (Buizert, 2013)	15
Table 2: Calibration results for permeameter models 2010 and 700 using packed glass beads	30
Table 3: Permeability results from testing the wedged membrane holder	32
Table 4: Microstructure parameters of 5 firn samples scanned twice on the microCT	38
Table 5: Accumulation/hiatus transitions and corresponding density measurements above (fine grain) and below (coarse grain) the transition depth	44
Table 6: Pore close-off modeled results for Vostok and Dome C, Antarctica	61

List of Figures

Figure 1: Schematic of an ice core	5
Figure 2: Diagram of firn from a high accumulation site with a high degree of layering and low accumulation site with little to no layering from Landais et al. (2006)	6
Figure 3: Mechanisms leading to sintering in polar firn (Chen 2008)	9
Figure 4: Measured density variability from Horhold et al. (2010) as a function of depth and mean density.....	10
Figure 5: $\delta^{15}\text{N}$ and $\delta^{40}\text{Ar}$ profiles at Megadunes, Antarctica (Severinghaus et al., 2010)	16
Figure 6: Diagram of an antidunes profile (Courville et al., 2007)	23
Figure 7: MODIS visible-band image composite where accumulation faces appear bright (left) and Radarsat Antarctic C band backscatter image where accumulation faces appear dark (right) (Courville et al., 2007)	23
Figure 8: Map of megadunes locations in Antarctica. The Megadunes site used for this study is in megadunes field closest to Vostok	25
Figure 9: Map of Antarctica indicating the location of WAIS Divide drilling site	26
Figure 10: Image of the model 2010 permeameter	28
Figure 11: Diagram of wedged holder and Megadunes firn core including inner base cylinder position	31
Figure 12: Schematic of the x-ray CT process from x-ray source to 3D representation (Landis and Keane, 2010)	33
Figure 13: Image of grey level thresholding and binarized firn 2D firn slice	34
Figure 14: Closed porosity correction of all samples	36

Figure 15: Ellipsoid of mean intercept lengths used to determine the degree of anisotropy	37
Figure 16: Image of WAIS Divide firn at a depth of 40.6m	40
Figure 17: Image of Megadunes firn at a depth of 41.2m	41
Figure 18: Density profiles of Megadunes and WAIS Divide from the surface to 80m ..	42
Figure 19: Density cross-over at WAIS Divide from the surface to 80m	43
Figure 20: Permeability profile of deep firn at WAIS Divide	45
Figure 21: Permeability profile of deep firn at Megadunes	46
Figure 22: Permeability and density profiles below 53m through pore close-off for Megadunes and WAIS Divide	47
Figure 23: Megadunes 3D pore space reconstruction where white is the pore phase	48
Figure 24: WAIS Divide 3D pore space reconstruction where white is the pore phase ..	48
Figure 25: Structure model index for WAIS Divide and Megadunes in deep firn	50
Figure 26: Surface to volume ratio for WAIS Divide and Megadunes in deep firn	51
Figure 27: Surface to volume ratio for WAIS Divide and Megadunes plotted against density in deep firn	52
Figure 28: Anisotropy for WAIS Divide and Megadunes	53
Figure 29: Total Porosity (% of sample) for Megadunes and WAIS Divide	54
Figure 30: Open Porosity (% of sample) for Megadunes and WAIS Divide	55
Figure 31: Closed Porosity (% of total porosity) for Megadunes and WAIS Divide	56
Figure 32: Profiles of log pore size, pore size, and number of pores greater than 0.001mm ³ in deep firn, 55m to 80m, for Megadunes and WAIS Divide	57
Figure 33: CPF for Megadunes and WAIS Divide	58

Figure 34: Permeability profile of Megadunes from 53m to 75m	60
Figure 35: Radar image of dune propagation through firn column down to 65m depth from the Megadunes site (Ted Scambos)	62
Figure 36: Wind crust frequency in surface snow pits, top 120 cm and in the firn column between 30m and 75m	63
Figure 37: Top 30m of Megadunes log of permeability profile with depth (Courville, PhD Thesis)	64
Figure 38: Relative Difference in Permeability on a half-meter scale from 55m through pore close-off	68
Figure 39: Density, permeability, and density/permeability relationship 30-36m and 55-80m	70
Figure 40: Density distribution of impermeable firn samples from the LID to the end of the LIZ where all samples are impermeable at Megadunes and WAIS Divide	73
Figure 41: Density cross-over of fine and coarse grain firn at WAIS Divide and deep firn permeability profile at WAIS Divide of fine and coarse grain firn	74
Figure 42: Measured and predicted permeability values and relative error for Megadunes and WAIS Divide	78

1 Introduction

When snow accumulates on land in very cold areas of the polar regions, where it never melts, it will gradually build up over time creating vast ice sheets that are able to store past climate signals in both the ice and the trapped air bubbles. To properly reconstruct and interpret climatic conditions of Earth's past, it is first necessary to understand how these signals are recorded. Of vital importance is the process in which polar firn, the porous stage between snow and ice, acts as a filter on atmospheric signals. At a given depth in an ice core, the air trapped within the ice matrix will always be younger than the ice due to the porous nature of the firn and the ability for atmospheric air to diffuse quickly to the base of the firn column. This age difference, commonly referred to as the gas age/ice age difference (Δ age), holds the key to understanding the phasing between climate signals such as temperature, reconstructed from the ice phase, and carbon dioxide concentrations, reconstructed from the gaseous phase. It is important to understand how current local climate influences the microstructure of the firn, the gas transport properties through the firn column, and at what depth and density pore close-off takes place. Knowledge of firn behavior under present climate conditions will enable better modeling of how the firn evolved and trapped air in the past; specifically during glacial periods and glacial-interglacial transitions.

Firn, characterized by its complex porous layered nature, consists of multiyear snow compacting and sintering due to overburden pressure. Densification and compaction of the firn continues until pores are sealed off from one another as bubbles by the surrounding ice. Due to the porous nature of the firn atmospheric air can diffuse to the base of the firn column on a decadal time scale (Schwander et al., 1997, Sowers et al.,

1992, Bender et al., 1997, Severinghaus et al., 2001, Kaspers et al., 2004). As the porosity of firn decreases with depth the controlling gas transport mechanisms also change (Sowers et al., 1992). Near the surface of the ice sheet, where firn is very porous convection is possible through wind pumping. Below the convective zone is the diffusive zone where molecular diffusion dominants gas transport. As the firn increases in density and pores become smaller and more segregated horizontal impermeable layers start to form initiating the lock-in zone. Within the lock-in zone, the air ages at the same rate as the surrounding ice and advection is the main transport mechanism. The length and presence of each of these zones varies from site to site depending on the local climate. This site to site variability and resulting microstructure differences that dictate gas transport and bubble entrapment in polar firn are not well understood. Due to this lack of knowledge, firn air models and firn densification models are calibrated to present day climate conditions and have a finite range under which they will produce accurate results. In order to extrapolate these models, beyond present day conditions, to extreme conditions found in glacial periods, the role of firn microstructure on pore close-off must be better understood.

This thesis focuses on the process of pore close-off and the evolution of microstructure in deep firn at two Antarctic sites, WAIS Divide and Megadunes. WAIS Divide was chosen because it is the current U.S. deep drilling location for the ice coring community, hence findings could have immediate impact on ice core interpretation. WAIS Divide has high snow accumulation and does not experience snow melt; its local climate conditions are similar to those at Summit, Greenland, where the GISP2 ice core was drilled. The Megadunes site captures an extreme end of present day climate

conditions due to its very low accumulation rate, cold temperatures, and high winds (Severinghaus et al., 2010). Stratigraphy, bulk density, and permeability measurements are done in conjunction with x-ray computed tomography to better understand the relationships between grain size, density, permeability, and pore structure. The overarching goals of this thesis are to

1. Characterize the lock-in zone at WAIS Divide and Megadunes
2. Understand how the physical signature of antidunes propagate down the firn column
3. Relate bulk properties to microstructure characteristics in deep firn
4. Provide insight into how local accumulation and temperature effects pore close-off

2 Background

2.1 Pore Close-off

2.1.1 The Lock-in Zone

Sometimes referred to as the non-diffusive zone, the lock-in zone (LIZ) exists at the bottom of the firn column ending at the firn-ice transition. The lock-in depth (LID), the depth at which the first horizontal impermeable layers of firn impede gas transport with the overlying atmosphere, marks the beginning of the lock-in zone. The close-off depth (COD), the depth where all pores are closed in both the horizontal and vertical directions, marks the end of the lock-in zone.

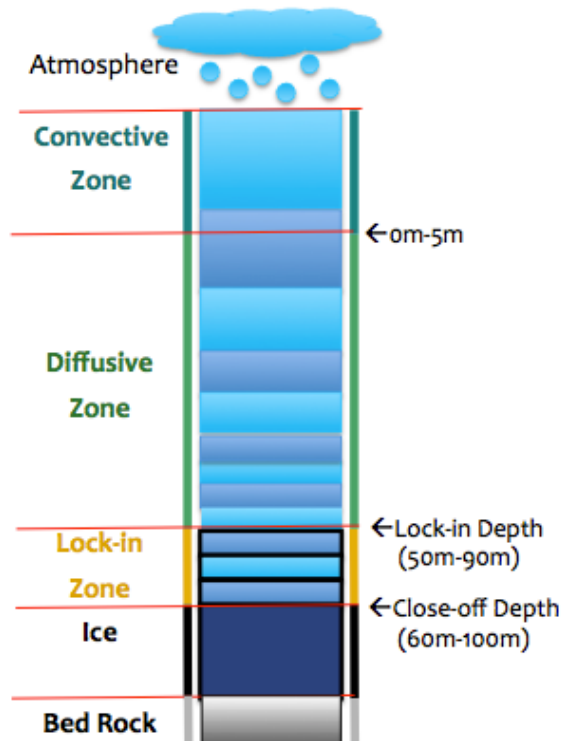


Figure 1. Schematic of an ice core. Note: Not to scale due to emphasis on the firn column including gas transport zones and important lock-in zone definitions.

As air ages at approximately the same rate as the surrounding ice matrix below the LID, the LID is critical for determining (Δ age). In addition, the length of the lock-in zone, is important for understanding the age spread of air trapped within bubbles at a given depth. While a small volume percentage of pores close above the lock-in zone the bulk of pore close-off happens between the LID and the COD.

2.1.2 Parameters Influencing of Pore Close-off

The depth of the LID and the length of the LIZ vary from site to site depending on local climate. Typically warm temperatures correspond to a shallow LID while cold temperatures lead to a deeper LID. Accumulation rate tends to have a direct relationship with LID depth where an increase in accumulation rate results in a deeper LID (Landais et al., 2006). Accumulation rate also influences the length and presence of the LIZ. According to Landais et al., (2006), an increase in accumulation rate will lead to an increase in the length of the LIZ.

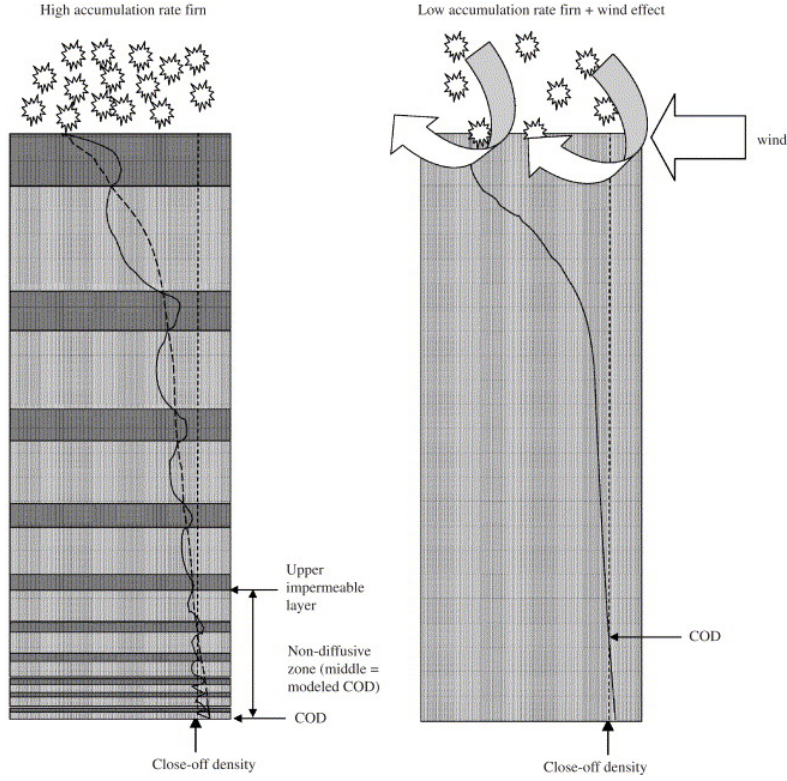


Figure 2. Diagram of firn from a high accumulation site with a high degree of layering (left) and low accumulation site with little to no layering (right) from Landais et al. (2006).

The assumption in the study by Landais et al. (2006) is that density variability associated with higher accumulation rates due to differences in winter and summer snow deposition is thought to propagate down the firn column and these layers will achieve pore close-off at different depths due to density variability, figure 2. To further understand the role of surface density variability and density variability at depth, Horhold et al. (2011) examined 16 high resolution density profiles of both Arctic and Antarctic firn. For all sites, a minimum in density variability was found at $\sim 0.60\text{-}0.65 \text{ g}\cdot\text{cm}^{-3}$ beyond which the variability increased again with depth until reaching a second minimum beyond the firn-ice transition. An inverse relationship was found where high accumulation rate leads to less density variability at the surface of the firn but greater variability at LIZ depths. Low

accumulation rates lead to higher density variability in surface firn but low variability at LIZ depths. The findings by Horhold et al. (2011) support those by Landais et al. (2006) in which low accumulation sites tend to have small to no lock-in zone while high accumulation sites have large lock-in zones.

2.1.3 Firn Densification Models and Pore Close-off

The ability to accurately reconstruct past close-off depths based on temperature and accumulation rate of a site is necessary for constraining Δ age. The Herron and Langway (1980) model examined density profiles of 17 polar sites covering both high and low accumulation rates from Greenland and Antarctica. The Herron and Langway model is commonly used to approximate the density profile of a given site but it does not account for the layered nature of the firn. A second model was developed by Martinerie et al. (1992), in which the mean pore close-off density is calculated based solely on the average temperature of a given site. Other studies have been done to better parameterize firn densification to include heat diffusion (Goujon et al., 2003) and the layered nature of the firn (Mitchell et al., 2013). Currently, the LID is characterized as the first layers of firn to reach a site specific pore close-off density that ranges between 13% and 21% total porosity depending on temperature and accumulation rate (Goujon et al., 2003). Firn densification models by Herron and Langway (1980), Barnola et al. (1991), Arnaud et al. (2000), and Goujon et al. (2003), are either entirely empirical or semi-empirical with calibrations dependent upon current climate condition of polar ice coring sites. These models also assume steady-state firn densification. While the firn densification models work reasonably well at predicting present day lock-in depths (LID), they produce large

uncertainties outside of their calibration range (Landais et al., 2006, Severinghaus et al., 2010). No densification model accounts for the porosity cross-over and how firn microstructure at depth may influence pore close-off.

2.2 Densification of Firn

While the firn column can be divided into zones based on the dominating gas transport mechanisms it can also be divided into sections based on the dominating densification mechanisms. Traditionally critical densities have been designated at $0.55 \text{ g}\cdot\text{cm}^{-3}$ and $0.83 \text{ g}\cdot\text{cm}^{-3}$ (Herron and Langway, 1980, Barnola et al., 1991). At densities above $0.55 \text{ g}\cdot\text{cm}^{-3}$ the major mechanism of densification is particle rearrangement and grain settlement (Herron and Langway, 1980). Between $0.55 \text{ g}\cdot\text{cm}^{-3}$ and $0.83 \text{ g}\cdot\text{cm}^{-3}$ the densification rate is slower and driven by a variety sintering mechanism. At densities greater than $0.83 \text{ g}\cdot\text{cm}^{-3}$ bubble compression drives densification until the maximum density of glacial ice is reached of $\sim 0.91 \text{ g}\cdot\text{cm}^{-3}$.

Snow deposition on the surface of an ice sheet will quickly undergo destructive metamorphism; where snowflake structure becomes more rounded and spherical (Colbeck, 1983). After this process the densification slows and temperature gradient induced vapor transport causes grain coarsening in the upper meters of the firn column. The lower the accumulation rate, the longer the residence time, the coarser the grains will become (Albert et al., 2004). In general, an increase in temperature will cause an increase in the rate of vapor transport while a decrease in temperature will slow vapor transport, the larger the temperature gradient, the quicker firn will metamorphisize (Alley, 1988). While grains are coarsening due to thermal gradients they are also settling

and compacting. At a density of $0.55 \text{ g}\cdot\text{cm}^{-3}$ the grains are thought to have reached their maximum packing arrangement (Herron and Langway, 1980).

Sintering of firn grains involves multiple mechanisms, figure 3, including three from surface sources; surface diffusion, vapor diffusion, two from grain boundary sources; grain boundary diffusion and lattice diffusion, and one from a dislocation source; lattice diffusion (Swinkels and Ashby, 1980).

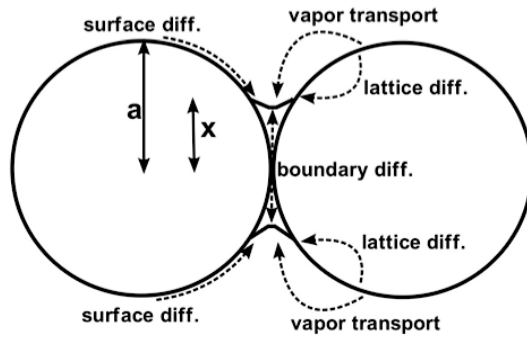


Figure 3. Mechanisms leading to sintering in polar firn (Chen 2008).

At densities between $0.55 \text{ g}\cdot\text{cm}^{-3}$ and $0.83 \text{ g}\cdot\text{cm}^{-3}$ the dominating mechanism for sintering is unclear and Freitag et al. (2004) postulated that the mechanisms act differently on fine grained and coarse grained layers.

A complicating factor of firn densification is the layered nature of polar firn where high and low density layers exist in close proximity to one another. This causes a unique situation where individual firn layers will reach the above critical densities at a variety of depths. Constraining firn densification through bulk density measurements does not always capture the true behavior of polar firn. Recently high resolution density

profiles have enabled a better understanding of how local density and centimeter scale density variability influence the firn densification process (Horhold et al., 2011).

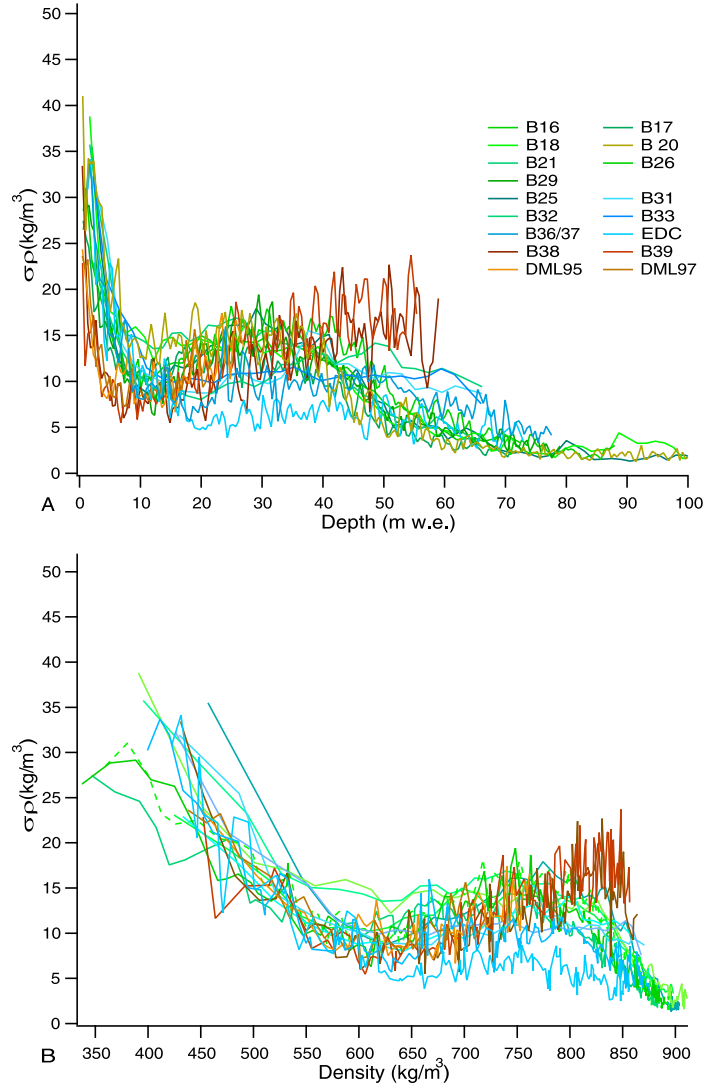


Figure 4. Measured density variability from Horhold et al. (2011) as a function of depth (top) and mean density (bottom). Note the minima in density variability at 0.60-0.65 $\text{g}\cdot\text{cm}^{-3}$.

From analyzing 16 various sites the critical densities of $0.55 \text{ g}\cdot\text{cm}^{-3}$ and $0.83 \text{ g}\cdot\text{cm}^{-3}$ are not as prevalent as previously thought. A new mimima in density variability, eluded to in

previous studies, is established to take place between $0.60\text{ g}\cdot\text{cm}^{-3}$ and $0.65\text{ g}\cdot\text{cm}^{-3}$, indicative of different rates of metamorphism between coarse grained and fine grained firn (Horhold et al., 2011). Horhold et al. (2012) postulated that the minima and second variability maxima may be due to the presence of impurities, specifically calcium, in the firn, rather than grain size.

2.3 Gas Transport in Porous Polar Firn

2.3.1 Permeability and Diffusivity

Simple relationships for permeability through porous media can also be applied to polar firn. Darcy's Law can be used to either model permeability via Lattice Boltzmann techniques (Courville et al., 2010, Freitag et al., 2002) or it can be applied to directly measure the permeability of discrete firn samples (Albert et al., 2000, Rick and Albert, 2004, and Courville, 2007). Darcy's Law is as follows:

$$v = (k/\mu) * (dP/dx) \quad (3)$$

where k is the permeability constant, μ is the air viscosity, dP is the pressure differential, dx is the height of the sample and v is the flow velocity. Freitag et al. (2002) found that permeability fits open porosity using a power law function with an exponent of 2.1.

Permeability of polar firn has a large influence on whether or not a specific site will have a convective zone, and if a convective zone is present how deep it will penetrate into the firn column. Courville et al. (2007) correlated the large convective zone at Megadunes, Antarctica to high permeability in the surface firn. A current study by Adolph et al. (in progress) has shown a linear relationship exists between diffusivity and permeability in deep firn, including the lock-in zone, but a decoupling in the

transport properties exist at high open porosities towards the firn surface. Adolph et al. (in progress) also found that the power laws derived by Freitag et al. (2002) are not appropriate over the entire porosity range exhibited by polar firn when compared with direct measurements. A possibility for this mismatch may be due to firn samples originating from different sites in each study and microstructural difference may result in different gas transport properties at each site.

Diffusion in a porous media including polar firn follows Fick's Law:

$$J(z,t) = -D * \partial c(x,t) / \partial z + c(z,t) * u \quad (1)$$

where J is the gas flux, z is the depth, t is the time, c is the mixing ratio, D is the diffusion coefficient and u is the superficial gas velocity (where $u = s_{op} * v$ where s_{op} is the open porosity and v is the flow rate of the carrier gas) (Fabre et al., 2000). To obtain the effective diffusivity of a gas within a connected porous structure the following relationship is given by (Dullien, 1975):

$$D_x = s_{op} D_x^0 / \tau \quad (2)$$

Where D_x is the effective diffusivity of gas x , D_x^0 is the free air molecular diffusion coefficient and τ is the tortuosity of the pore structure. Several studies have directly measured the effective diffusivity of gases within the porous matrix of polar firn (Schwander et al., 1988, Fabre et al., 2000, Adolph and Albert, 2013). The method used to measure diffusivity on individual firn samples by Schwander et al., (1988) and Fabre et al. (2000) required the use of both a tracer gas and carrier gas. To obtain the gas diffusivity, measurements of an eluting peak of the tracer gas were made over a variety of flow rates and extrapolated to zero. After measuring gas diffusivities a relationship with total porosity was developed in which diffusivity drops to zero below 0.12 porosity but

shows no site to site variability. Fabre et al. (2000) found that measurements of diffusivity on discrete firn samples do not capture the entire diffusive behavior of the firn through forward modeling. Note that both studies parameterize the effective diffusivity and tortuosity of the firn with total porosity and give no indication as to how open versus closed porosity may influence the relationship.

Adolph and Albert (2013) adapted techniques previously established for porous media, such as soil, to use on polar firn where diffusivity is measured directly using an inert tracer gas, SF₆. The study applied a numerical solution for Fick's second law of diffusion to calculate the diffusivity of the tracer gas. Further work by Adolph et al. (in progress) has shown promise in using direct diffusivity measurements on discrete samples in capturing the true diffusive behavior of polar firn at Summit, Greenland. Freitag et al. (2002) and Courville et al. (2010) applied Lattice Boltzman modeling for diffusion on three dimensional reconstructions of polar firn. Freitag et al. found that effective diffusivity followed open porosity in a power law function with an exponent of 3.4.

Molecular diffusion in polar firn leads to gravitational and thermal fractionation of heavy isotopes and molecules. The dominating process in polar firn is gravitational fractionation enriching heavy isotopes towards the base of the firn column. Gravitational fraction follows the barometric equation and can be written:

$$\delta_{\text{grav}} = \exp[gz\Delta M/RT] - 1 \times 10^3 \quad (4)$$

Where δ_{grav} is the enrichment of an isotope relative to atmospheric concentrations, g is the gravitational constant, z is the depth, ΔM is the mass difference, R is the gas constant, and T is the temperature of the gas (Craig et al., 1988). While the effect is smaller,

thermal fractionation may play an important role during abrupt climate change when a larger temperature gradient exists in the firn column than exists under stable climate conditions (Severinghaus et al., 2001, Weiler et al., 2009).

2.3.2 Firn Air Measurements

Air existing in the open porosity of the firn column can be sampled strategically with depth as firn cores are drilled for a variety of reasons. While the firn air is typically only a few decades old at the base of the firn column, some recent anthropogenic changes in atmospheric gases such as mercury (Fain et al., 2008) can be seen and quantified. The major focus of firn air campaigns is understanding how firn can smooth and alter atmospheric signals before air is entrapped in bubbles and many studies throughout Antarctica and Greenland have been conducted (Clark et al., 2007, Buzert et al., 2011, Kawamura et al., 2006, Schwander et al., 1993, Witrant et al., 2011, Etheridge et al., 1996, Trudinger, 2001, Severinghaus et al., 2010, Severinghaus et al., 2001, Fabre et al., 2000, and Battle et al., 2011). A wide range of sites, with a variety of temperatures and accumulation rates, have been studied and were succinctly summarized by Buzert (2013) in the following table.

Site	Location		Altitude (m a.s.l.)	P (hPa)	T (°C)	A (cm ice year ⁻¹)	CZ depth (m)	z _{cod} (m)	Year(s) sampled	Main references
Northern Hemisphere										
Devon Isl.	75.3° N	82.1° W	1929	792 ^a	-23	30	~0 ^b	59	1998	FIRETRACC, Clark et al. (2007)
NEEM	77.4° N	51.1° W	2484	745	-28.9	22	4	78	2008, 2009	Buizert et al. (2012)
NGRIP	75.1° N	42.3° W	2917	691	-31.1	19	1-2 ^c	78	2001 ^d	CRYOSTAT, Kawamura et al. (2006)
Summit	72.6° N	38.4° W	3214	665	-31.4	23	~0 ^b	80	1989, 2006	Schwander et al. (1993), Witrant et al. (2011)
Southern Hemisphere										
Berkner Isl.	79.6° S	45.7° W	900	895 ^e	-26	13	<2 ^c	64	2003	CRYOSTAT
DE08-2	66.7° S	113.2° E	1250	850	-19	120	0 ^b	85	1993	Etheridge et al. (1996)
DML ^f	77.0° S	10.5° W	2176	757 ^e	-39	7	<5 ^c	74	1998	FIRETRACC
Dome C	75.1° S	123.4° E	3233	658 ^e	-54	2.7-3.2	2 ^c	100	1999	FIRETRACC
Dome Fuji	77.3° S	39.7° E	3810	600	-57.3	2.3-2.8	9	104	1998	Kawamura et al. (2006)
DSSW20K	66.8° S	112.6° E	1200	850	-21	16	4	52	1998	Trudinger (2001)
H72	69.2° S	41.1° E	1241	857	-20.3	33	2	65	1998	Kawamura et al. (2006)
Megadunes	80.8° S	124.5° E	2880	677	-49	~0 ^g	23	68	2004	Severinghaus et al. (2010)
Siple Dome	81.7° S	148.8° W	620	940	-25.4	13	<2 ^b	57	1996, 1998	Severinghaus et al. (2001)
South Pole	90.0° S		2840	681	-51	8	<2 ^b	123	1995-2008 ^h	Severinghaus et al. (2001)
Vostok	78.5° S	106.8° E	3471	632	-56	2.4	13 ^b	100	1996	Fabre et al. (2000)
WAIS-D	79.5° S	112.1° W	1766	780	-31	22	3	76.5	2005	Battle et al. (2011)
YM85	71.6° S	40.6° E	2246	730	-34	17	14 ⁱ	68	2002	Kawamura et al. (2006)

Unless indicated otherwise, values can be found in the main references or references therein (last column).

^aHuber et al. (2006).

^bSeveringhaus et al. (2010).

^cLandais et al. (2006).

^dThere were two separate NGRIP firn air campaigns in 2001 (J. Schwander, personal communication, 2011).

^eCalculated from the altitude using the pressure-altitude relationship over Antarctica from Stone (2000).

^fAlso referred to as BAS depot (Landais et al., 2006). Note that the location differs from that of the EDML ice core.

^gThe long-term average accumulation estimate is 2.5 cm ice year⁻¹. Sampling was done during an accumulation hiatus.

^hFirn air was sampled in 1995, 1998, 2001, and 2008.

ⁱHigh wind speeds at the site cause the unusually thick CZ.

Table 1. Summary of firn air sampling sites and characteristics. From Buizert, Studies of Firn Air, Encyclopedia of Quaternary Science, 2013.

As can be seen in table 1, accumulation rate and temperature play an important role in the size and presence of the convective zone and the close off-depth.

When no convective zone is present, gaseous isotopes such as $\delta^{15}\text{N}$ will fractionate according to the barometric equation until the LID. Therefore, the diffusive column height is reflected in the amount of gravitational fractionation at the base of the firn column (Severinghouse et al. 2010). The convective zone thickness can be

determined from firn air measurements by extrapolating gravitational fractionation in the diffusive zone to isotope concentrations equal to those found in the atmosphere.

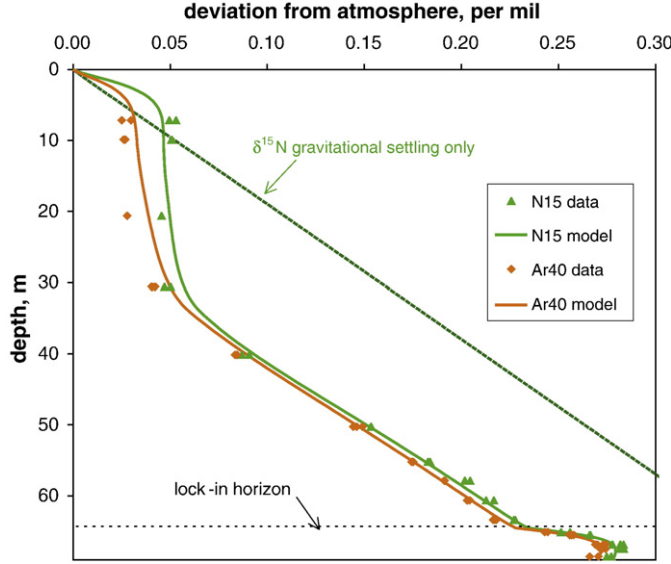


Figure 5. $\delta^{15}\text{N}$ and $\delta^{40}\text{Ar}$ profiles at Megadunes, Antarctica (Severinghaus et al., 2010)

For example, Severinghaus et al. (2010) found that a convective zone of 23m exists at Megadunes, Antarctica. The start of the lock-in zone, the lock-in depth, is defined by firn air measurements as the point in which $\delta^{15}\text{N}$ deviations no longer follow the barometric equation. The end of the lock-in zone, the close-off depth, is said to be approximate to the depth at which air can no longer be sampled from the firn column (Buizert, 2013).

2.3.3 Firn Air Models

To apply what has been learned through firn air measurements, firn gas transport models have been developed. These models usually estimate the diffusivity profile of a given site using the Schwander et al. (1988) parameterization for tortuosity and effective diffusivity and then apply inverse modeling with firn air measurements to tune the diffusivity profile to a specific site (Buizert, 2013). As many inverse models use only

one trace gas the solutions are not well constrained (Buizert et al., 2012). Recent studies by Buizert et al. (2012) and Witrant et al. (2011) use multiple tracer gases to better constrain the firn air models. While multiple tracers greatly improves inverse firn air models, inverse modeling is not possible for past firn columns where it is impossible to know what the firn air concentration profiles were.

Firn air models are commonly used to find the age distribution of the air trapped at a given depth, to reconstruct recent atmospheric concentrations from firn air measurements, and to estimate the diffusive column height from $\delta^{15}\text{N}$ measurements of deep ice cores. Constraining the age distribution at the base of the firn column establishes the resolution limit of atmospheric signals (Buizert et al., 2012, Schwander et al., 1993, Trudinger et al., 1997). Modeling of the age distribution is typically done on the air within the open pore space of the firn column but has also been done on the air trapped within the closed bubbles of deep polar firn (Mitchell et al., 2013). These models are also used on reconstructed firn columns of the past to estimate the smoothing that occurred in the atmospheric signals recorded in the bubbles of deep ice cores. Along with the age distribution at a given depth, modeling of firn air transport within modern firn columns enables the reconstruction of recent atmospheric concentration profiles for a variety of gases. Studies have been done to reconstruct a multitude of gas concentrations including carbon dioxide, methane, ethane, mercury, and carbon monoxide among others (Etheridge et al., 1996, Braunlich et al., 2001, Aydin et al., 2011, Fain et al., 2009, Assonov et al., 2007).

Perhaps the most important application of firn air models is reconstruction of past diffusive column heights through $\delta^{15}\text{N}$ measurements from deep ice coring records.

Modeled diffusive column height can be used to estimate the LID during past climatic conditions and consequently constrain the gas age/ice age difference. A short coming of estimating LID from just the diffusive column height is a lack of knowledge about the length of both the convective and diffusive zones (Schwander et al., 1997).

2.4 Data-model Mismatch

As atmospheric air diffuses through the firn, the firn acts as a filter on the air as the microstructure compacts and sinters, in effect causing the trapped air to always be younger than the surrounding ice. Determining the gas age/ice age difference (Δage) is highly dependent upon the local climate, specifically the accumulation rate and temperature, at the time of entrapment. Current firn densification models by Herron and Langway (1980), Barnola et al. (1991), Arnaud et al. (2000), and Goujon et al. (2003), are calibrated to be dependent upon current climate condition of polar ice coring sites. These models also assume steady-state firn densification. While the firn densification models work reasonably well at predicting present day lock-in depths (LID), they produce large uncertainties outside of their calibration range. The uncertainties lead to a data-model mismatch during glacial and glacial-interglacial transitions between the LID predicted with firn densification models and the LID reconstructed from air isotopic composition, $\delta^{15}\text{N}$ measurements (Landais et al., 2006, Loulergue et al., 2007, Capron et al., 2012, Dryefus et al., 2010, and Parrenin et al., 2013). To properly address Δage accurately constraining both firn densification models and the use of $\delta^{15}\text{N}$ as a proxy for LID is vital.

2.5 Microstructure of Polar Firn

The microstructure of polar firn influences both the densification and gas transport processes of firn. Original methods of microstructure characterization involved image analysis of two dimensional thin slices (Alley et al., 1982). While 2D reconstructions give a reasonable indication of pore structure, development of 3D imaging techniques fully captures the complex nature of polar firn. Three dimensional analysis has been done on firn cores through reconstruction of thin slices (Freitag et al., 2002) and microcomputed tomography. Although x-ray computed tomography is well established in soil science (Taina et al., 2008), initial application to polar firn has only happened in the last 10-15 years (e.g. Coleou et al., 2001; Freitag et al., 2004;; Schneebeli et al., 2004). A number of studies have been done using x-ray computed tomography to examine the microstructure of polar firn from the surface through the firn-ice transition. These studies have focused primarily on understanding how microstructure differences between fine grained and coarse grained firn influences the densification rate of polar firn (Freitag et al., 2004, Lomonaco et al., 2011, Fujita et al., 2009). Other studies include the influence of microstructure, either from thin sections or x-ray computed tomography on the permeability of firn at the top of the firn column (Albert et al., 2004, Courville et al., 2007, Rick and Albert, 2004).

Fujita et al. (2009) focused on microstructure to understand how insolation influences the firn and how the insolation signal is expressed at depth. The study used bulk density measurements at 3mm resolution, 3D reconstructions of the pore space and the qualitative measure of permeability to characterize the firn. Fujita et al. (2009) found that initially high density layers were less dense than initially low density layers in deep

firn. The initially high density layers were also found to be more permeable at depth through qualitative measurements of permeability. They conclude that diffusion at the base of the firn column depends on the extent of summer insolation and subsequent alternation of microstructure characteristics at Dome Fuji (Fujita et al., 2009). Freitag et al. (2004) also follows the metamorphism of fine grained and coarse grained layers from the surface of the firn to the firn ice transition from core B27 drilled in Greenland. The study found that coarse grained layers densify at a quicker rate than fine grained layers, postulating that the sintering mechanisms involved in densification probably act differently on differently sized grains. Interestingly the pore size of both fine grained and coarse grained layers decreases at very similar rates at equivalent depths in the firn column. Quicker rates of densification in coarse grained firn leads to a porosity (or density) cross-over in which initially dense layers at the surface become the less dense layers in deep firn. This regime shift implies that pore close-off should occur first in fine grained firn layers if pore close-off is microstructure dependent (Freitag et al., 2004).

Lomonaco et al. (2011) specifically addresses the fine grained firn layers at Summit, Greenland from the surface of the firn down to 90m just past the firn-ice transition. The study found that the majority of pores in fine grained layers close below 65m starting just above the LIZ defined through firn air measurements that starts at 69m. The microstructure of the fine grained layers decreased in structure model index, a measure of concavity/convexity of the ice structure, until a value of -9, indicative of ice surrounding spherical air bubbles (between 70-90m). Around 25-35m the structure model index becomes negative in response to the ice structure transforming from convexly shaped ice grains surrounded by air to a concavely shaped ice structure

surrounding the interstitial pore space. For both the Freitag et al. (2004) and Lomonaco et al. (2011) studies, permeability measurements were not done on the samples and thus knowledge of which layers, fine or coarse reach pore close-off first is unknown.

In depth studies of how microstructure affects gas transport in the near surface of firn columns have been conducted by Albert et al. (2004), Rick and Albert, (2004), Courville et al. (2007), and Horhold et al. (2009). The major focus of these studies was to relate permeability measurements to microstructural characteristics developed through either two dimensional or three dimensional firn reconstructions. Albert et al. (2004) found a correlation between low density, coarse grained firn layers and an increase in permeability in the top meter of firn at Megadunes, Antarctica. Comparison with other polar sites showed that the unique hiatus sites found on the leeward face of the dunes consisting of very large coarse crystals caused much higher permeability values than those found at higher accumulation sites such as Summit, Greenland ($24\text{cm}\cdot\text{a}^{-1}$ w.e.) and Siple Dome, Antarctica ($11\text{cm}\cdot\text{a}^{-1}$ w.e.). Further examination of the top two meters of the firn at Megadunes, at both a hiatus and an accumulation site, were conducted by Courville et al. (2007). The microstructure at the accumulation site consisted of very fine grained wind pack with many wind crusts, in direct contrast to the microstructure at the hiatus site which consisted of large coarse grains. While density profiles of both locations were similar, with the hiatus site being slightly less dense at multiple depths, the permeability of the hiatus site was noticeably higher than the permeability at the accumulation site. This study provided a direct link between microstructure and gas transport in the surface firn at Megadunes which has been linked to the large convective zone that exists down to 23m at the Megadunes site.

Rick and Albert, (2004) also related microstructure characteristics to the permeability profiles of multiple shallow cores from the 2000 ITASE expedition. This study highlighted the impact of accumulation rate on permeability by showing a direct connection between an ENSO-induced accumulation rate change and a marked increase in permeability at depth where this event is currently located in the firn column. The increase in permeability corresponds to an increase in grain size of both summer and winter layers due to an increased residence time at the surface of the ice sheet.

Another study done by Horhold et al. (2009) on near surface firn microstructure and permeability also found evidence for accumulation rate impacting the grain size of polar firn in the top 2.5m. The increase in grain size at the surface keeps an enduring signature as it is buried within the firn column. This enduring signature continues to affect gas transport at depth. It was found that the lower the accumulation rate, the longer the residence time in the upper 2.5m of firn, the larger the grains, the higher the permeability within the firn (Horhold et al., 2009). In general for all of the permeability studies done on near surface firn, permeability increases to a maximum around 2.5m depth as snow grains coarsen and then decreases as sintering and densification processes control firn metamorphism. Fluctuations and differences between sites in permeability profiles are likely due to changes in accumulation rate and other local climate signals. How microstructure continues to influence polar firn permeability down the firn column until complete pore close-off has not yet been established.

2.6 Megadunes

Megadunes, or antidunes, are unique to very low accumulation sites and occupy large areas of interior East Antarctica.

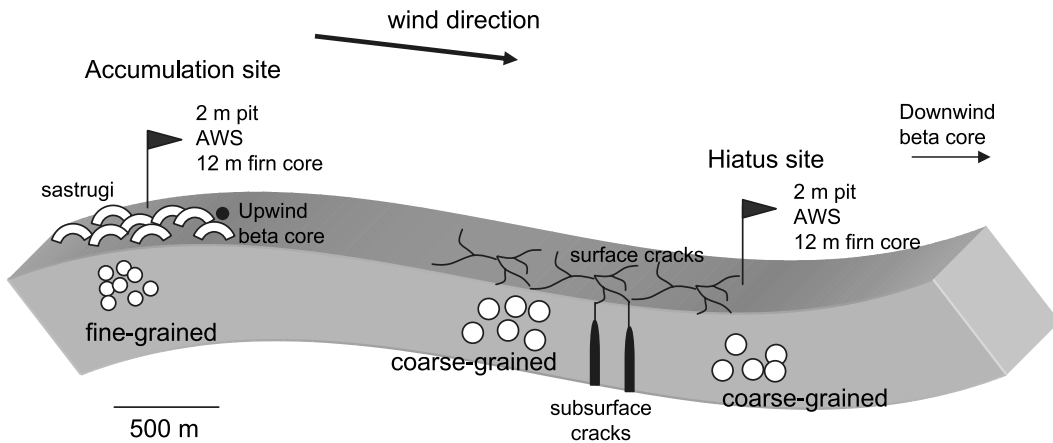


Figure 6. Diagram of an antidunes profile (Courville et al., 2007).

They are characterized as long wavelength (2-5 km) and short amplitude (2-4 m) with accumulation occurring primarily on the windward dune face, accumulation sites, which can be covered in large sastrugi. As the leeward dune faces, hiatus sites, have little to zero accumulation they are sastrugi-free with extensive depth hoar (Frezzotti et al., 2002). From satellite imagery megadunes have been found to migrate upwind at $10 \text{ to } 20 \text{ m}\cdot\text{a}^{-1}$ (Fahnestock et al., 2000).

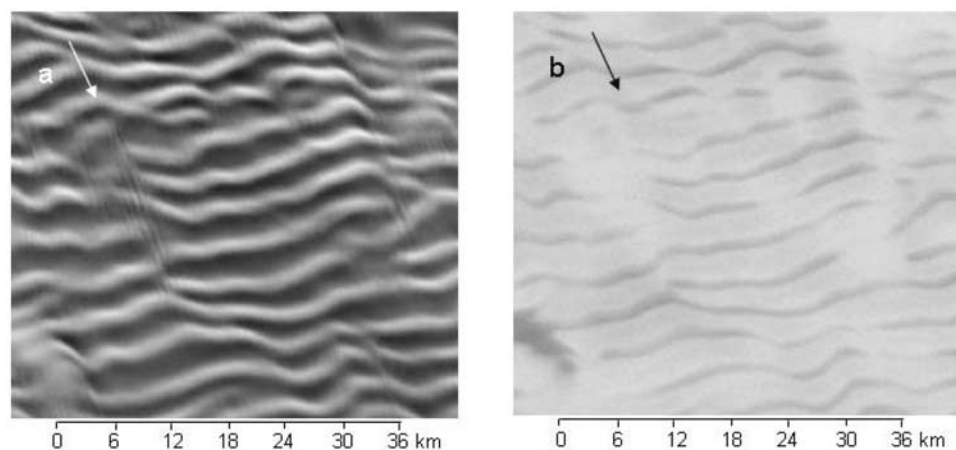


Figure 7. MODIS visible-band image composite where accumulation faces appear bright (left-a) and Radarsat Antarctic C band backscatter image where accumulation faces appear dark (right-b) (Courville et al., 2007).

The presence of Megadunes and their migration upwind slowly buries past dune faces that are preserved in the firn column. The presence of hiatus sites, with large coarse firn grains increases the permeability of the surface firn (Courville et al., 2007). The direct result of an increase in permeability, significantly higher than other present day firn sites, is deep convection.

2.7 Site Characteristics

2.7.1 Megadunes

Measurements of firn air and extraction of a firn core from a megadunes site in East Antarctica were accomplished at an undisturbed site in December 2004-January 2005 at 80.77914° S, 124.48796° E. Courville et al., 2007 thoroughly describes the site details and near-surface measurements, and Severinghaus et al 2010 describes firn air results.. The average temperature at the site is -49° C with an accumulation rate less than 4cm weq yr⁻¹. In-situ firn air measurements at Megadunes done by Severinghaus et al. (2010) indicate a LIZ from 64.5m to 68.5m. The convective zone at Megadunes is notably very large reaching a depth of ~23m (Severinghaus et al., 2010).

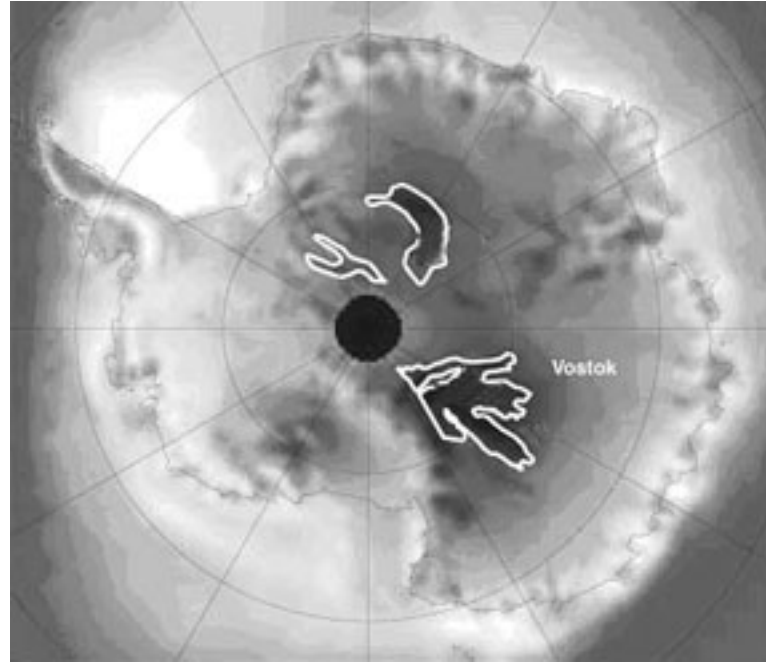


Figure 8. Map of megadunes locations in Antarctica. The Megadunes site used for this study is in megadunes field closest to Vostok.
http://nsidc.org/cryosphere/antarctica/megadunes/megadunes_camp.html

2.7.2 WAIS Divide

Firn core, WDC05C, was retrieved from a previously undisturbed site at 79.46300° S 112.12317° W near the WAIS Divide ice coring site for firn air measurements in December 2005-January 2006. (Battle et al., 2011). The mean annual temperature at the site is -31°C and the average accumulation rate is 22cm yr^{-1} ice-equivalent (Banta et al., 2008). The accumulation rate and average temperature at the site are both significantly higher than those at the Megadunes location. From in-situ firn air measurements done by Battle et al. (2011) a LIZ exists from approximately 66m to 76.54m. Similar to other high accumulation sites, the convective zone is small, likely ranging between 1.4m and 5.2m in depth (Battle et al., 2011).

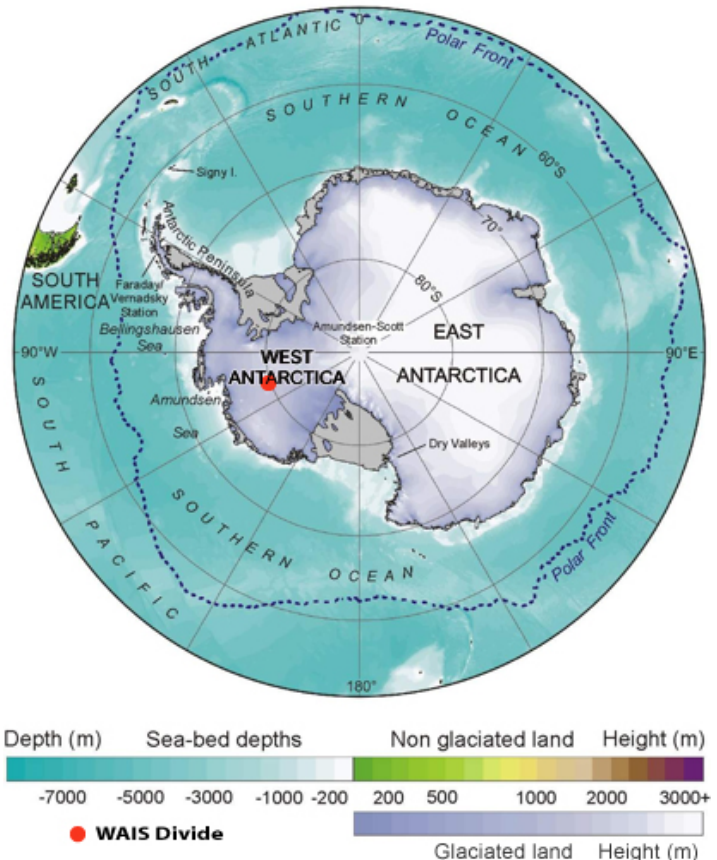


Figure 9. Map of Antarctica indicating the location of WAIS Divide drilling site.
<http://www.waisdivide.unh.edu/science/index.shtml>

3 Methods

3.1 Visual Stratigraphy

Visual stratigraphy was observed using a backlit light table in a cold room at the Cold Regions Research and Engineering Laboratory in Hanover, NH. Meter long core sections were placed on the light table where grain size and wind crusts were recorded to the 1 mm scale. Grain size was qualitatively described using a five tier scale from coarse to fine for each meter length section. Coarse and fine were defined relative to other layers within the meter long section. Samples of 5-10 cm of similar grain size were cut for further analysis. Emphasis was put on obtaining a single homogenous layer of firn per sample whenever possible, in order to facilitate comparisons of the properties with quantitative microscopy results.

3.2 Bulk Density

Bulk density measurements made on the same done 5-10 cm resolution samples using volumetric measurements and the mass of the sample.

$$\rho_s = 4 * m_s / (\pi * d_s^2 * h_s) \quad (5)$$

where ρ_s is the density of the sample, m_s the mass, d_s the diameter, and h_s the height. As a slice taken from the Megadunes firn core for isotopic analysis, volumetric calculations were adjusted for the change in shape accordingly. Error in density measurements was small with less than 0.5% standard deviation for 10 repeat measurements on a single sample. Broken or chipped pieces were not reported in bulk density or permeability measurements.

3.3 Permeability

3.3.1 Permeability of Firn Samples

Permeability measurements were made using the methods developed by Albert et al., 2000, and used for example in Rick and Albert, 2004, and Courville, 2007. Using a custom apparatus that had been verified on glass beads, air was drawn through a firn sample, and the associated flow rate and pressure drop across the sample were measured, along with temperature and barometric pressure. A variety of flow rates were employed. For each flow rate and associated pressure drop recorded, the permeability was obtained using Darcy's law. Flow rates of air through the samples were kept within the laminar flow regime where Darcy's Law holds true.

$$v = (k/\mu) * (dP/dx) \quad (6)$$

where k is the permeability constant, μ is the air viscosity, dP is the pressure differential, dx is the height of the sample and v is the flow velocity.



Figure 10. Image of the model 2010 permeameter.

Before measurements were taken the permeameter was calibrated using glass bead samples until measured permeability of the glass beads was within the bounds of literature values on packed glass bead permeability. Ten measurements with ten different flow rates were done on each sample and usually fell within 5-10% of one another. At very low permeabilities fewer measurements were done on each sample due to the low flow rates needed to stay within the laminar flow regime and the range of the pressure transducer. During measurements, as permeability decreased and the differential pressure across the firn sample increased larger range pressure transducer of 15" and 30" were used. The minimum permeability measured on a firn sample with the 30" pressure transducer was $0.01 \times 10^{-10} \text{ m}^2$ and all samples whose measurements fell below the range of the 30" pressure transducer range were considered impermeable for the purposes of this study.

3.3.2 Calibration of the Permeameter with Glass Beads

Calibration was done on the 2010 and 700 model permeameters through glass bead testing. Three glass bead samples of 0.75mm, 1mm and 3mm diameter beads were assembled. Assembly of samples consisted of pouring beads into 3-inch diameter cylinders with the inner edges coated in clay to reduce edge-affects from increased gas flow between the cylinder side and bead edges (Adolph and Albert 2013). The cylinders had a packing factor for a randomly packed specimen between 0.35 and 0.40 total porosity.

Permeability of randomly packed spherical particles can be determined theoretically through the Carmen-Kozeny relationships based on total porosity and particle size. The Carmen-Kozeny relationship is as follows:

$$k = \epsilon^3 * d^2 / (180 * (1 - \epsilon)^2) \quad (7)$$

Where k is the permeability constant, d is the diameter of the spherical particle and ϵ is the porosity of the specimen (Garboczi, 1990).

Permeability of each glass bead sample was taken ten times on each permeameter for the 0.1" and 0.5" pressure transducers. An exception was made for the 0.75mm and 1mm glass beads, these were measured only with the 0.5" pressure transducer because the pressure differential across the bead sample was beyond the 0.1" pressure transducer's range. Inclusion of both pressure transducers was done to assess the limits of their range for accurate permeability measurement. The results of the tests are displayed in Table 2. Along with permeability measurements on the glass bead samples, approximations of permeability for spherical beads using the Carman-Kozeny relationship are also displayed.

d_{bead} (mm)	k_{meas} 2010 model (.1"/.5" Pxducer)	k_{meas} 700 model (.1"/.5" Pxducer)	k_{Pred} Carman-Kozeny (.35-.40 porosity)
3	54.75/51.88	52.88/49.75	50.74-88.89
1	---/6.54	---/7.11	5.64-9.88
0.75	---/4.62	---/4.70	3.17-5.56

Table 2. Calibration results for permeameter models 2010 and 700 using packed glass beads.

For all sized glass beads and appropriate pressure transducers, the measured values fell within the literature values for packed glass beads with porosity between 0.35 and 0.40. As bead size and permeability decreased the measured values were in the central range of literature values. Note that the 0.5" pressure transducer was appropriate for the 1mm and

0.75mm glass beads while the 0.1" pressure transducer was appropriate for the 3mm glass beads. While all three sizes of glass beads have similar porosities, the size and tortuosity of the pores play an important role in permeability magnitude.

3.3.3 Wedged Membrane Testing for Megadunes Permeability

The permeameter holder developed by Rick and Albert (2004) uses a cylindrical firn sample. The firn core taken at the Megadunes site had a segment removed for oxygen isotope analysis and a new, wedged holder was developed for permeability measurements. The following diagram shows the top down view of the new holder and the Megadunes firn core dimensions as well.

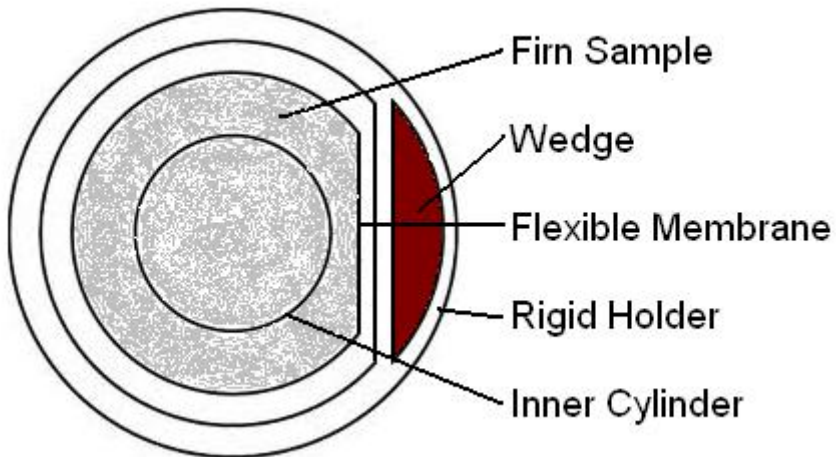


Figure 11. Diagram of wedged holder and Megadunes firn core including inner base cylinder position.

The base that supports the firn specimen has two concentric cylinders in which only the inner flow, and inner pressure differential of the sample is measured to avoid edge effects between the membrane and the sample. While a portion of the outer cylinder was not

covered by Megadunes firn samples, the entire surface area of the inner cylinder was covered ensuring flow and pressure differential measurements were entirely within the firn sample. Tests were done on three firn samples that were initially cylindrical and then cut to the shape of the Megadunes firn core to test the reliability of the wedged holder. Permeability measurements were done twice for each firn sample under both conditions; whole and cut. The results of these measurements are displayed in Table 3 and show changes in permeability between cut and uncut samples below error estimates of a single whole sample of 5-10%.

Sample ID	Whole 1	Whole 2	Average Whole	Cut 1	Cut 2	Average Cut	Relative Diff. %
SUFA07-29-2	10.5	9.3	9.9	9.5	10	9.75	1.51
SUFA07-31-2	7.4	8.9	8.15	8.3	7.5	7.9	3.06
SUFA07-32-2	7.1	7.3	7.2	7.4	6.7	7.05	2.08

Table 3. Permeability results from testing the wedged membrane holder.

3.4 Micro Computed Tomography

3.4.1 Micro Computed Tomography Acquisition and Settings

Firn microstructure properties were obtained using x-ray micro computed tomography (microCT). A Skyscan 1172 model microCT was used in a cold room. Scans were run at 40kV with a 250 μ A current intensity. For each scan, a rotation step of 0.7° was used with the specimen completing 180° rotation. 275 shadow images were obtained and reconstructed using Skyscan's NRecon software for two dimensional slice reconstruction. The resolution of the images obtained is 14.8 μ m in which each voxel obtained represents a three dimensional cube with 14.8 μ m side length. Firn samples were cut to 10mm width x 10mm width x 15mm height from the center of the 5cm-10cm samples used in density and permeability measurements. Samples were taken from the

center of the larger firn sample to minimize any metamorphism the outer edges of the sample may have gone through during storage. The volume of interest analyzed for microstructure properties was 538 x 538 x 673 voxels or 8mm x 8mm x 10mm in size.

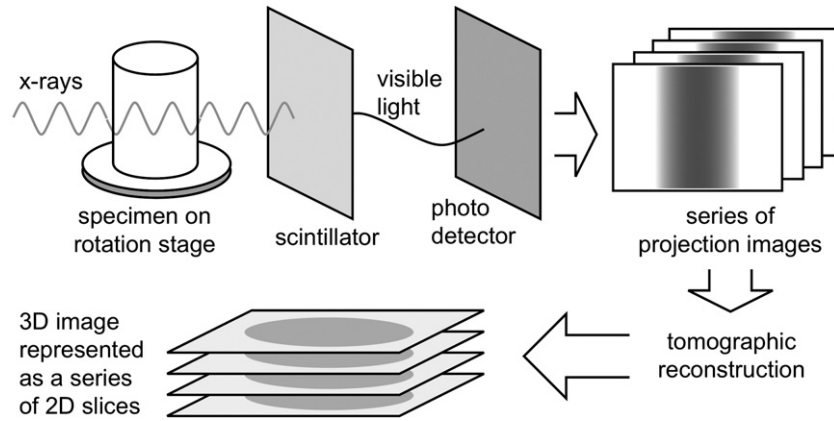


Figure 12. Schematic of the x-ray CT process from x-ray source to 3D representation (Landis and Keane, 2010).

Tracking the CT process from start to finish, figure 12; an x-ray source produces x-rays for a given set-up which pass through the sample to the detector which relays the information in the form of projected images for each step in rotation to a computer program that reconstructs these images into two-dimensional slices piled together into a three-dimensional representation of the sample object (Landis and Keane, 2010).

Beam hardening and ring artifacts during acquisition can limit the resolution and accuracy of quantitative analysis of x-ray computed tomography. Beam hardening is the result of lower energy x-rays attenuating more than higher energy x-rays as they pass through the sample. The increase in attenuation of these lower energy x-rays causes the center of the sample to appear dark while the edges appear significantly brighter (Ketcham and Carlson, 2001). The gradation in grey scale from the center of the image

to the edge can cause issues with phase identification. To reduce acquisition defects, beam hardening was set to 40% for all samples and ring artifact reduction was done manually for each sample within the NRecon reconstruction software.

Reconstruction of images applies tomographic reconstruction mathematics, a principle based on solving a series of equations obtained for a given intensity at a specific position in the sample object (Landis and Keane, 2010). Each rotational angle of the CT scanner produces a projection of the object unique to that angle. Combining each projection and solving the series of equations, enables the intensity to be found at each position. These intensities are given grey scale values for each voxel and are used to produce the two-dimensional slices. Because these intensities are related to the attenuation coefficient of the material, distinguishing between phases of differing attenuation coefficients (densities) becomes a matter of thresholding. For thresholding 256 grey levels were used and a thresholding value of 89 was set between the air and the ice phase.

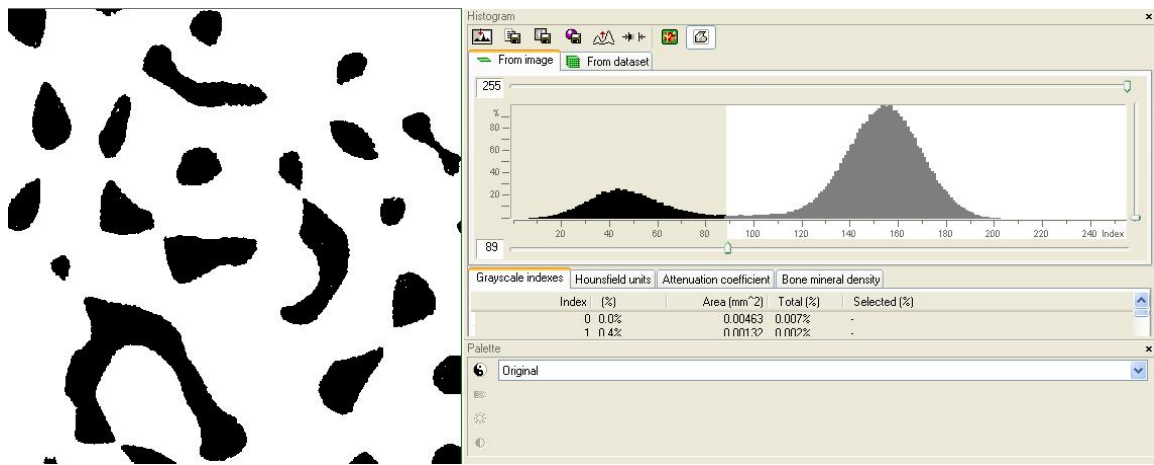


Figure 13. Image of grey level thresholding and binarized firn 2d firn slice.

The large difference in linear attenuation coefficients (x-ray absorption) between ice and air enables a simple thresholding limit to be used to binarize the images. To reduce noise

and minimize falsely counting incorrectly binarized voxels as pores or small ice clusters, all white specs less than 25 voxels surrounded by black voxels were removed and vice versa. Image analysis on both the ice phase and pore phase was done to obtain the microstructure properties of both the ice structure and pore structure of the firn sample.

3.4.2 Microstructural Properties

The microstructural properties, derived using Skyscan's CTan software, include total porosity, open porosity, closed porosity, structural model index, surface to volume ratio, and anisotropy. Microstructural properties were obtained on both the ice and pore phases. The total porosity of the sample is determined by counting the total number of voxels present for the ice phase and dividing that by the total number of voxels within the region of interest. Open porosity is defined as any pore that intersects with the edge of the region of interest at least once. From the total and open porosity values, the closed porosity of a sample can quickly be determined through subtraction. To account for closed pores that were cut during sample preparation, pore size distribution was determined for all of the samples where the majority of closed pores had volumes of 1mm^3 or less. Through individual object analysis all pores with a center within 0.62mm (the radius of a 1mm^3 spherical pore) of the edge of the region of interest were considered closed. Open porosity and closed porosity were then adjusted accordingly for each sample. Corrections to closed porosity were small, Figure 14.

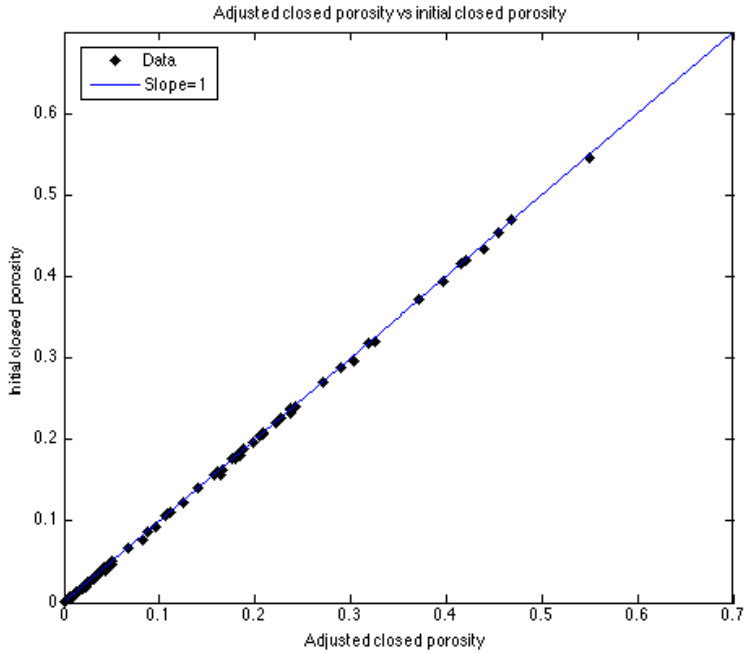


Figure 14. Closed porosity correction of all samples

The structure model index, (SMI), gives an estimation for the type of shape present in the analyzed phase. SMI values of 0, 3 and 4 correspond to an ideal plate, cylinder, and sphere respectively. Calculation of SMI follows that developed by Hildebrand et al. (1997) in which one voxel thickness is added to the surface of the phase analyzed. SMI is then calculated as follows:

$$SMI=6*(S'*V)/S^2 \quad (8)$$

Where S' is the artificially increased surface area, S is the original surface area, and V is the initial volume of the analyzed phase. For convex shapes, SMI is positive while concave structures have negative SMI values. The surface to volume ratio, (S/V), gives the ratio of the analyzed phase surface area to the volume of the phase in three dimensions. It gives estimation of how tortuous an object is where a low S/V indicates

less complexity in shape than a high S/V (Morphometric parameters measured by SkyscanTM CT- analyser software, Bruker-MicroCT CT-Analyser, <http://www.skyscan.be>).

Anisotropy is a measure of alignment or three-dimensional symmetry within the region of interest. The value of anisotropy is determined using the mean intercept length; the length of a line traveling through an object divided by the number of times the line crosses the phase being analyzed. The higher the mean intercept length the more the object is aligned in a single direction indicating a high degree of anisotropy.

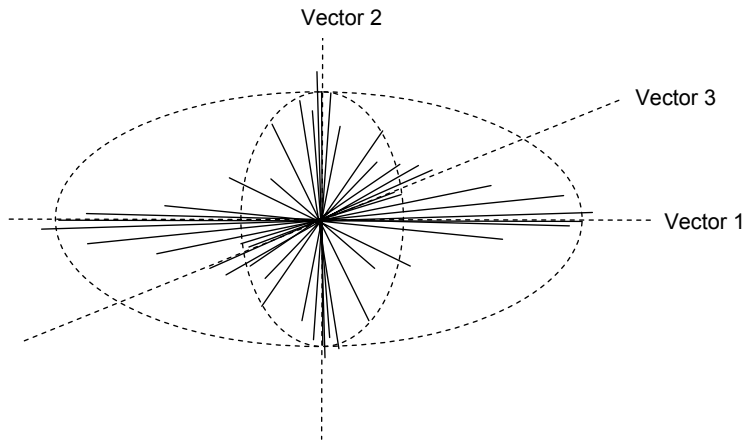


Figure 15. Ellipsoid of mean intercept lengths used to determine the degree of anisotropy (Morphometric parameters measured by SkyscanTM CT- analyser software, Bruker-MicroCT CT-Analyser, <http://www.skyscan.be>).

The mean intercept length is found at many 3D angles within the region of interest and each MIL is plotted to create an ellipsoid. The ellipsoid seen in figure 14 is described using an orthogonal tensor whose maximum and minimum eigenvalues are used to determine the degree of anisotropy as follows:

$$DA = (1 - [\min_{\text{eigenvalue}} / \max_{\text{eigenvalue}}]) \quad (9)$$

Where the degree of anisotropy (DA) ranges from a value of 1, totally isotropic to

infinity, totally anisotropic (Morphometric parameters measured by SkyscanTM CT-analyser software, Bruker-MicroCT CT-Analyser, <http://www.skyscan.be>).

When addressing error on parameters derived from microcomputed tomography analysis one has to consider multiple sources of error including measurement error, the natural variability in horizontal strata of the firn column and sufficient sizing of the analyzed firn specimen. A firn size of 8mm x 8mm x8mm has been determined to be sufficient in other studies (Coleou and others, 2001; Kaempfer and Schneebeli, 2007, Freitag et al., 2004, Courville et al., 2010). A limited number of samples were scanned twice and the results are shown in table 4.

Depth (m)	Total Porosity (total volume)			Open Porosity (total volume)			Closed Porosity (total porosity)		
	1	2	% Diff (rel)	1	2	% Diff (rel)	1	2	% Diff (rel)
MGDFA 64.98	8.81	8.31	5.67	7.37	6.77	8.14	0.16	0.19	13.47
MGDFA 69.49	8.07	7.64	5.36	5.88	5.94	1.03	0.27	0.22	18.17
MGDFA 70.61	7.65	7.51	1.78	6.07	6.14	1.24	0.21	0.18	11.76
WDC05C 64.26	12.08	12.04	0.32	11.55	11.48	0.61	0.04	0.05	6.31
Depth (m)	Structure Model Index SMI			Surface to Volume Ratio S/V			Anisotropy 1 to infinity		
	1	2	% Diff (rel)	1	2	% Diff (rel)	1	2	% Diff (rel)
MGDFA 64.98	2.21	1.95	11.89	10.88	11.02	1.26	1.24	1.32	6.82
MGDFA 69.49	2.59	1.89	26.98	9.16	9.26	1.08	1.32	1.48	12.00
MGDFA 70.61	2.39	1.99	16.92	9.04	8.68	4.00	1.39	1.21	12.76
WDC05C 64.26	1.67	2.35	41.00	10.83	10.38	4.11	1.21	1.17	2.95

Table 4. Microstructure parameters of 5 firn samples scanned twice on the microCT.

While the relative difference in total porosity, open porosity, closed porosity, surface to volume ratio, and anisotropy are generally below 15%, structure model index

shows higher variability. SMI is very dependent upon where the region of interest is placed and the number of pores that are dissected by it because it is a measure of pore convexity or concavity. The sample from WAIS Divide has the highest porosity and also the largest difference in structure model index. As SMI is an indicator of pore shape and is not used quantitatively for any other reason, these discrepancies are ignored. Differences and trends with both depth and between cores, in total porosity, open porosity, closed porosity and surface to volume ratio, are greater than 15% and are thus considered significant. Due to time constraints and error less than 15% in quantitative parameters, from the above 4 samples, the majority of samples were scanned once. Error bars are not included on microstructure parameters but are assumed to be less than 15% and likely within the natural variability of polar firn in a single horizontal layer. Error in an individual sample was been found to be $\leq 10\%$ for permeability measurements, and thus error over all measurements is of approximately the same magnitude.

4 Results

4.1 Stratigraphy

Firn is a layered, porous media and thus noting the stratigraphy profile of a given firn column is important for understanding how microstructure relates to bulk properties.

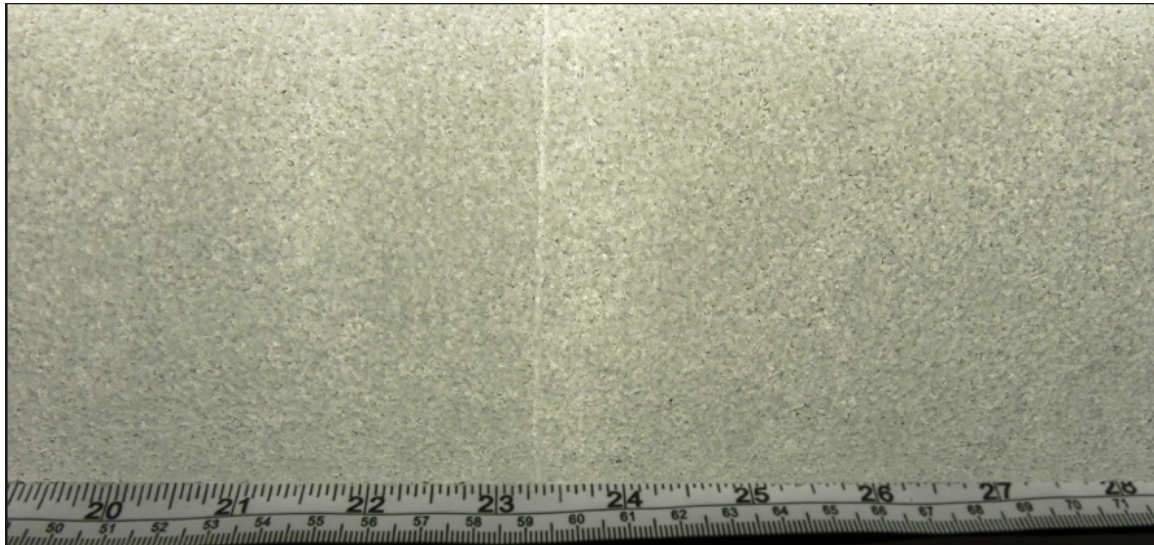


Figure 16. Image of WAIS Divide firn at a depth of 40.6m.

Centimeter scale layering can be seen in the WAIS Divide firn core at all depths. Figure 16, firn from 40.6m depth at WAIS Divide has alternating layers of fine grained and coarse grained firn as well as a wind crust in the center of the image.

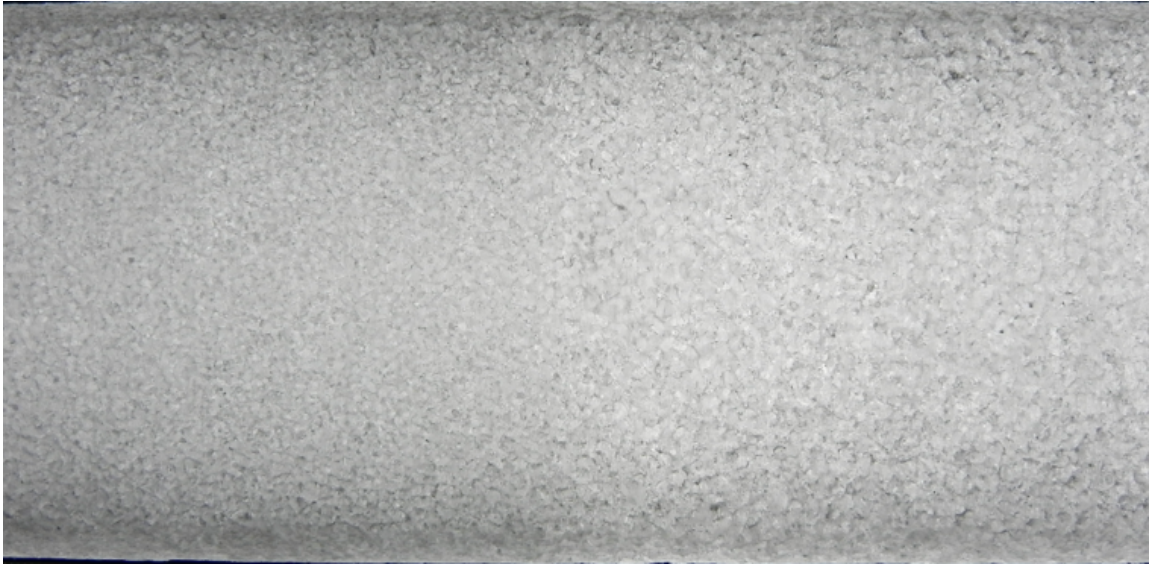


Figure 17. Image of Megadunes firn at a depth of 41.2m.

Figure 17 shows the abrupt switch from a past accumulation site to a past hiatus site at 41.2m depth for the Megadunes firn core. The past accumulation site consists of fine grained firn while the past hiatus site is made of coarse grained firn. Note the lack of layering in the sample other than the one transition. Megadunes firn has large coarse grains while WAIS Divide has finer smaller grains at equivalent depths (Figures 16 and 17). Another distinction between the Megadunes and WAIS Divide is the scale over which layering exists. At Megadunes, large sections of core, up to several meters long will be either predominately coarse grained or predominately fine grained. On the other hand, the firn at WAIS Divide has quick alternations, on the centimeter scale, between coarse grained layers and fine grained layers.

4.2 Density

A common practice in firn studies is measuring the density profile of the firn column. Density cross-overs within polar firn have been observed at multiple sites

including in Northern Greenland, Dome Fuji and Berkner Island in Antarctica, as well as many more (Freitag et al., 2004, Hori et al., 1999, Gerland et al., 1999, Horhold et al., 2011).

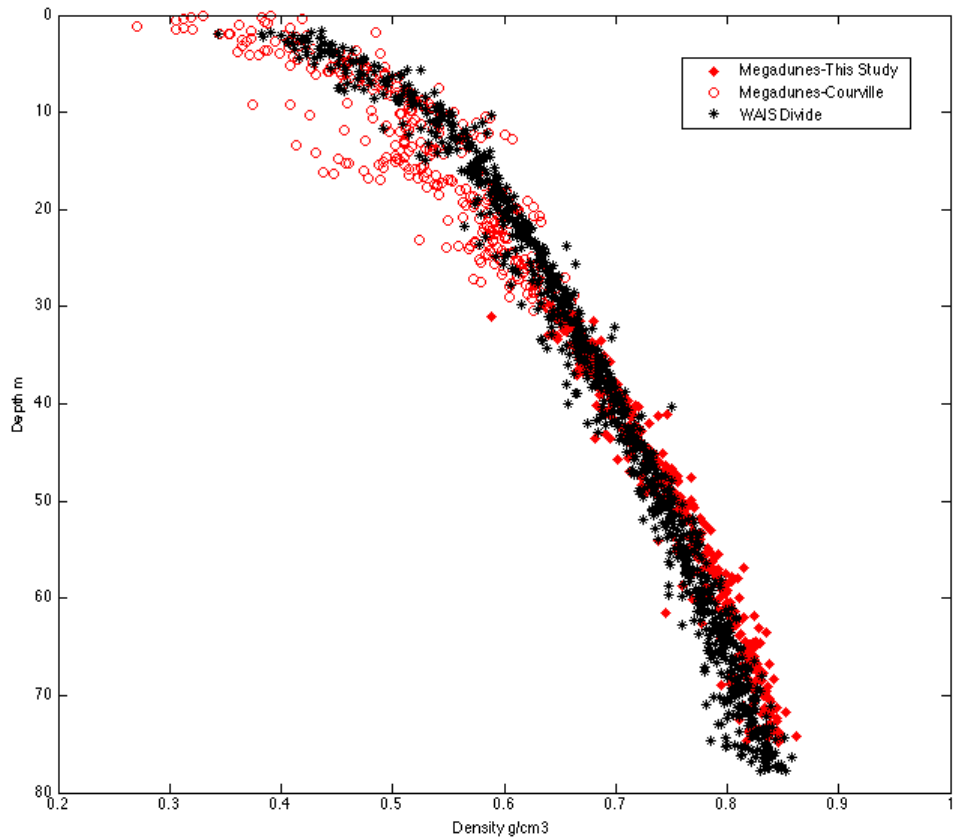


Figure 18. Density profiles of Megadunes (red diamonds) and WAIS Divide (black stars) from the surface to 80m.

Figure 18 shows the density profiles for both WAIS Divide and Megadunes. While Megadunes firn is initially less dense than the firn at WAIS Divide, it is more dense at the lock-in depth and pore close-off. Worth noting is that Megadunes firn consists of much coarser grains at depth than WAIS Divide firn and that Megadunes firn is more dense than WAIS Divide firn at depth.

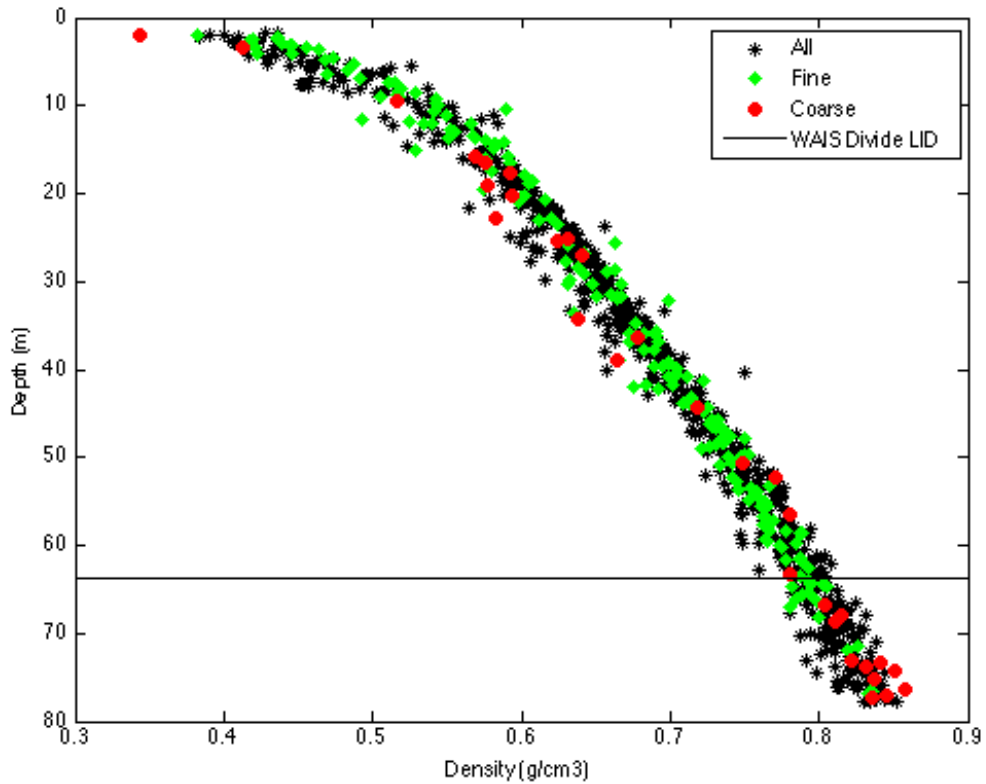


Figure 19. Density cross-over at WAIS Divide from the surface to 80m where fine grain (green diamonds), coarse grain (black stars), and all other samples (red circles).

Throughout the firn column, fine grained and coarse grained layers are determined visually based on their relative grain size to other firn layers in the surrounding one meter of firn. Plotted in figure 19 is the evolution of fine grained and coarse grained firn layers with depth at WAIS Divide. At WAIS Divide, initially dense layers correspond to fine grained firn at the surface, whereas at the bottom of the firn column, dense layers correspond to coarse grained firn. The exact location of the cross-over is difficult to pinpoint in figure 19. Higher resolution density measurements on the WDC06A core show the minima in density variability occurs around 30m at WAIS Divide (Kreutz et al., 2011).

Depth (m) accumulation to hiatus transition location	Density (g/cm ³) Accumulation (fine)	Density (g/cm ³) Hiatus (coarse)
14 ^a	~(0.57-0.60)	~(0.46-0.50)
23 ^a	~0.60	~0.57
36	0.68	0.66
42	0.73	0.71
53	0.78	0.76
60	0.80	0.78
65	0.82	0.81

*Below 65 m, dune transitions are close together and show no distinct pattern in density variability of coarse grained and fine grained layers. (^a Courville, PhD Thesis)

Table 5. Accumulation/hiatus transitions and corresponding density measurements above (fine grain) and below (coarse grain) the transition depth.

Megadunes firn exhibits no density cross-over between fine grained and coarse grained layers; the coarsest grain firn remains less dense than the finest grained firn from the surface through the LIZ. Firn with grains between the coarsest and finest layers at Megadunes have some density variability but not as extreme as the direct switch from the fine grains to the coarse grains. Table 5 summarizes dune transition locations where firn layers dramatically switch from dense fine grained layers to less dense coarse grain layers over several millimeters.

4.3 Permeability

While density gives the amount of mass present, permeability gives an approximation of the open pore space of a given porous media. Permeability measurements were done from approximately ten meters (53m at Megadunes and 55m at WAIS Divide) above the LID determined by firn air studies (Severinghaus et al., 2010, Battle et al., 2011).

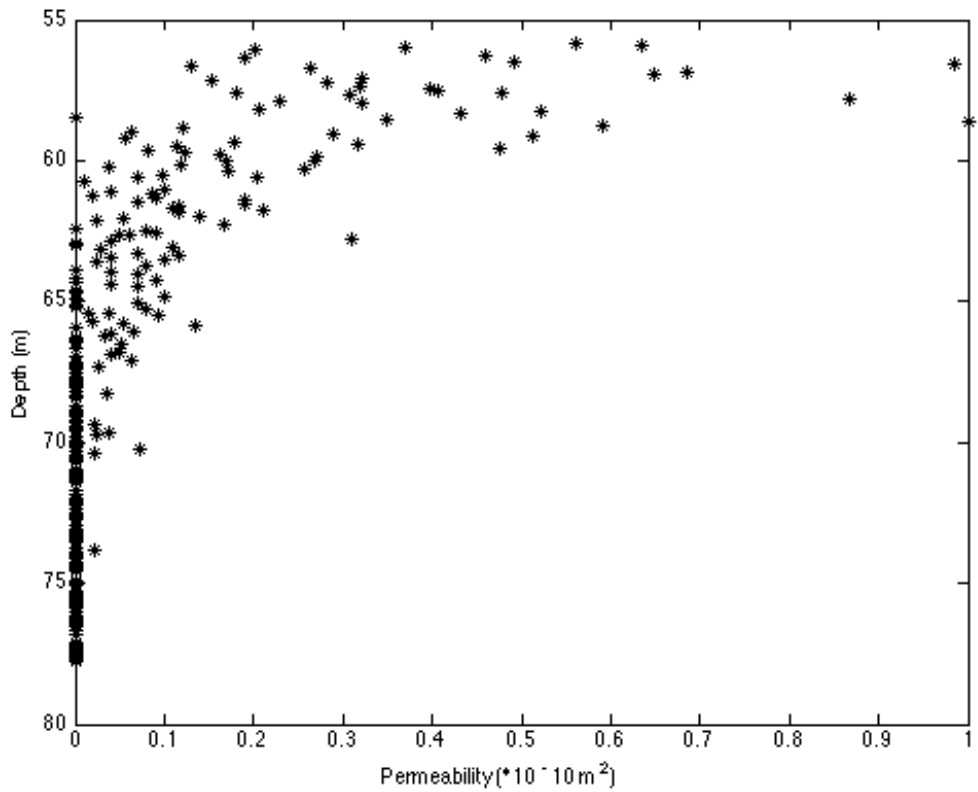


Figure 20. Permeability profile of deep firn at WAIS Divide

Firn air measurements give a lock-in depth at WAIS Divide between 66-68m (Battle et al., 2011). The lock-in depth determined through permeability measurements on individual firn samples for WAIS Divide is 63.85m, indicative of the depth at which several consecutive samples are impermeable. The first impermeable sample occurs a few meters above the LID at 58.47m. This depth is not considered the LID due to the three dimensionality of polar firn where one impermeable layer from a firn core may not be horizontally significant in nature.

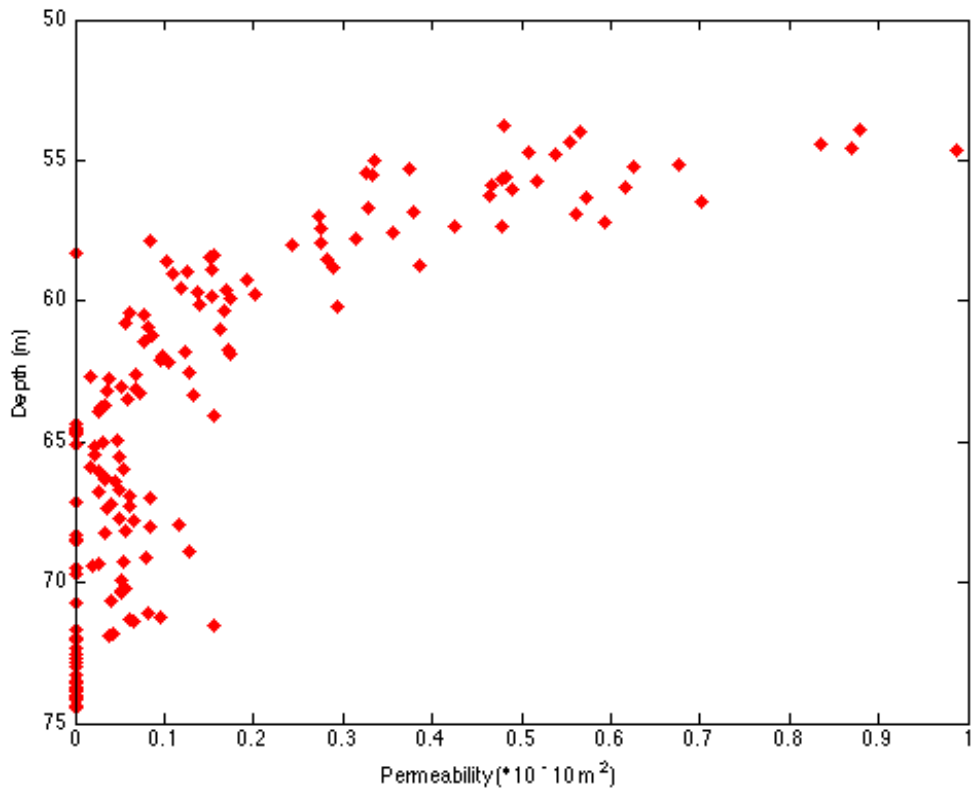


Figure 21. Permeability profile of deep firn at Megadunes

Firn air measurements produce a lock-in depth at 64.8m at Megadunes (Severinghaus et al, 2010). Permeability measurements of Megadunes firn indicate the LID at 64.37m almost perfectly aligned with the LID from firn air measurements. The first measured impermeable layers is found at 58.28m for Megadunes. As was previously mentioned for the permeability profile of WAIS Divide, a single impermeable layer is not considered horizontally significant in nature and thus not considered the LID.

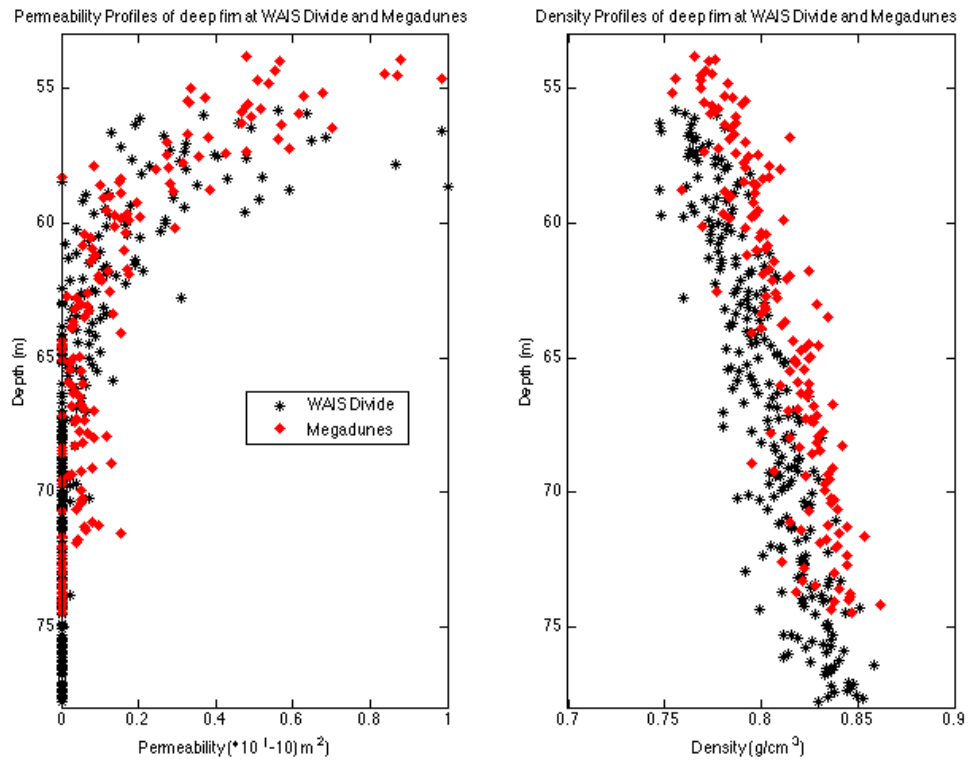


Figure 22. Permeability and density profiles below 53m through pore close-off for Megadunes (red diamonds) and WAIS Divide (black stars).

The permeability profiles of both Megadunes and WAIS Divide seen in figure 22, and plotted individually in figures 20 and 21, are of the same magnitude from 55m to the LID or start of the lock-in zone. Interestingly, the density profiles from the same depth interval show Megadunes firn to be consistently denser than WAIS Divide firn. The permeabilities within the lock-in zone at Megadunes have more scatter than the permeabilities of WAIS Divide within the lock-in zone. The lock-in zone at Megadunes is also shorter than the lock-in zone at WAIS Divide that extends to almost 75m. The similarities in permeability but differences in densities between both sites suggest the pore structure of the firn plays has an impact on gas transport properties within polar firn.

4.4 Microstructure

4.4.1 Visual 3D Reconstructions

Microstructure imaging helps to understand the reasons for different density and permeability profiles at Megadunes and WAIS Divide. Figures 23 and 24 display three-dimensional reconstructions obtained using microcomputed tomography. The width and thickness of the reconstructed firn cubes is 8mm while the height is 10mm.

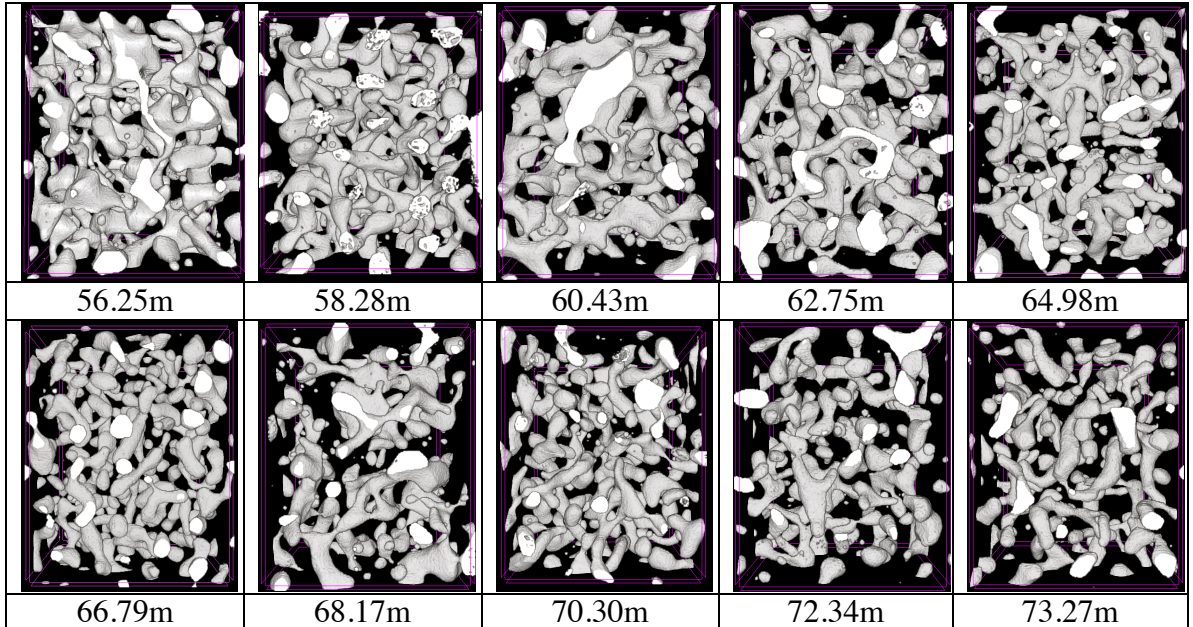
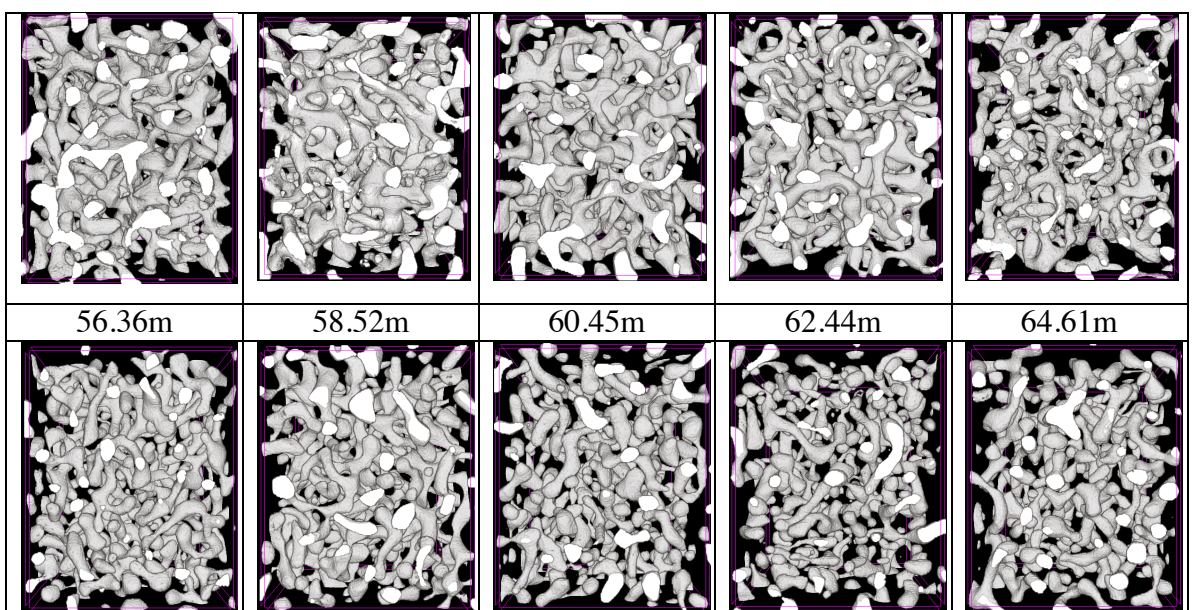


Figure 23. Megadunes 3D pore space reconstruction where white is the pore phase.



66.56m	67.38m	70.56m	73.51m	74.50m
--------	--------	--------	--------	--------

Figure 24. WAIS Divide 3D pore space reconstruction where white is the pore phase.

Visually Megadunes firn (Figure 23) has larger but less total pore space at an equivalent depth than WAIS Divide (Figure 24). The pore structure at WAIS Divide also looks more complex and divided. For both sites, total pore space decreases and the occurrence of bubbles increases with depth.

4.4.2 Microstructural Parameters

Microstructure analysis enables quantification and validation of differences in visual observations seen between the two sites. Microstructural parameters analyzed on the pore phase include structure model index (SMI), surface to volume ration (S/V), and anisotropy.

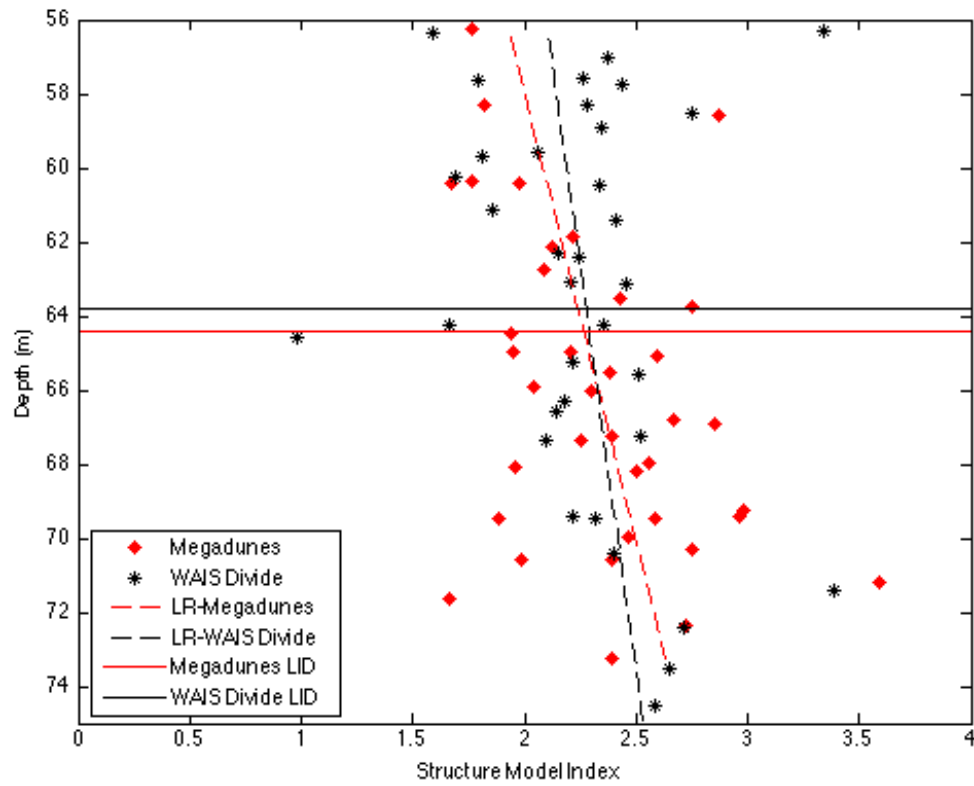


Figure 25. Structure model index for WAIS Divide (black stars) and Megadunes (red diamonds) in deep firn.

The SMI profile, an indicator of pore shape, is the same for Megadunes and WAIS Divide with depth. The pore structure at Megadunes and WAIS Divide (Figure 4) is primarily cylindrical at 55m with increasing SMI, evolving to spheres towards the firn-ice transition. A linear fit to the data shows a slightly steeper slope in SMI for Megadunes a sign that the pore structure at Megadunes may become spherical bubbles at a shallower depth than the pore structure at WAIS Divide.

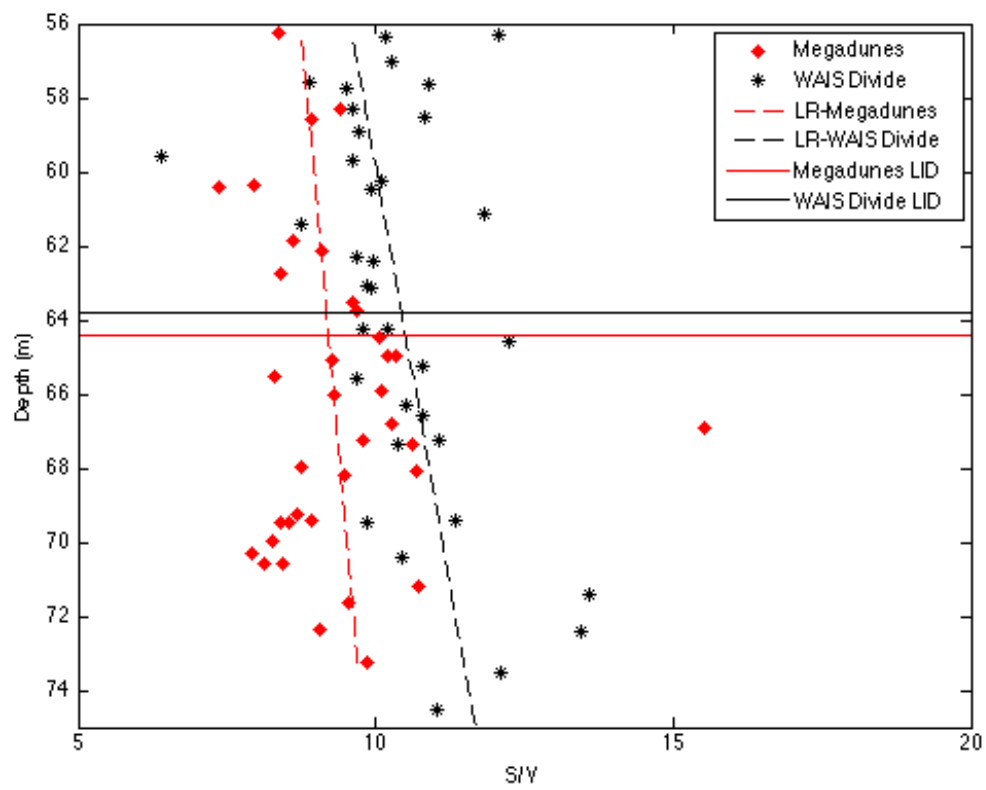


Figure 26. Surface to volume ratio for WAIS Divide (black stars) and Megadunes (red diamonds) in deep firn.

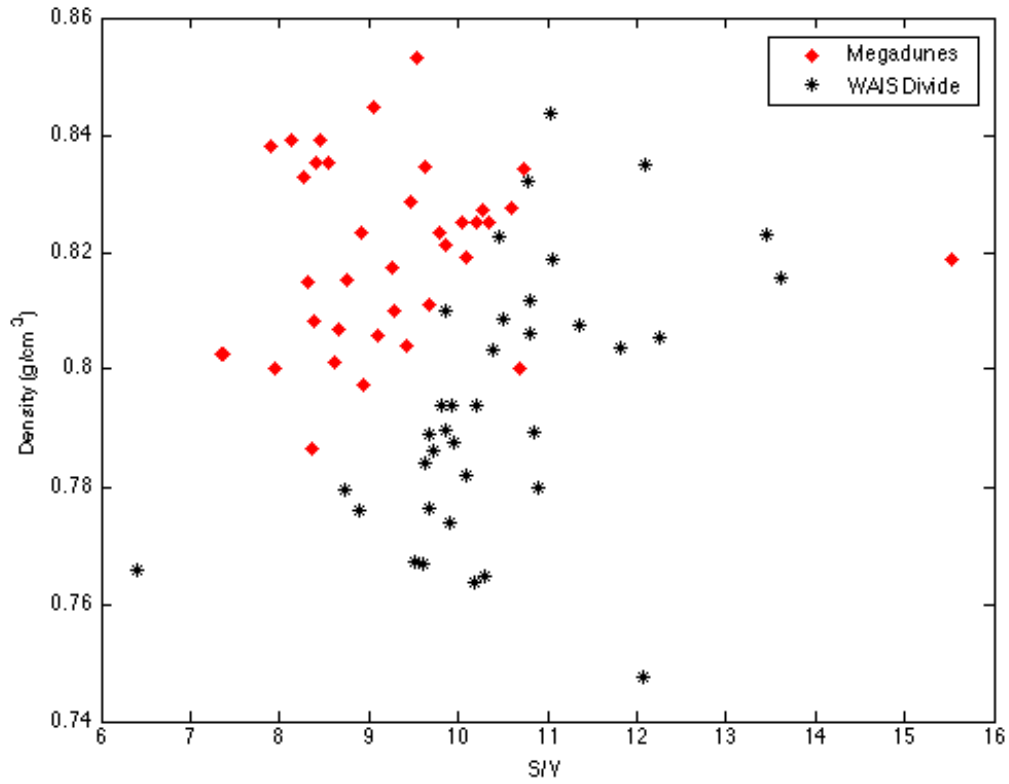


Figure 27. Surface to volume ratio for WAIS Divide (black stars) and Megadunes (red diamonds) plotted against density in deep firn.

Surface to volume ratio (S/V) characterizes the complexity of a structure and can serve as a proxy for tortuosity (Spaulding et al., 2011). Megadunes firn has consistently lower values of S/V than WAIS Divide indicating a less tortuous pore structure at a given depth (Figure 26). S/V at Megadunes is lower than at WAIS Divide at equivalent densities as well (Figure 27). Comparing S/V between the two sites, finding Megadunes firn to be less complex than WAIS Divide firn, confirms visual observations made on the 3D firn cube reconstructions.

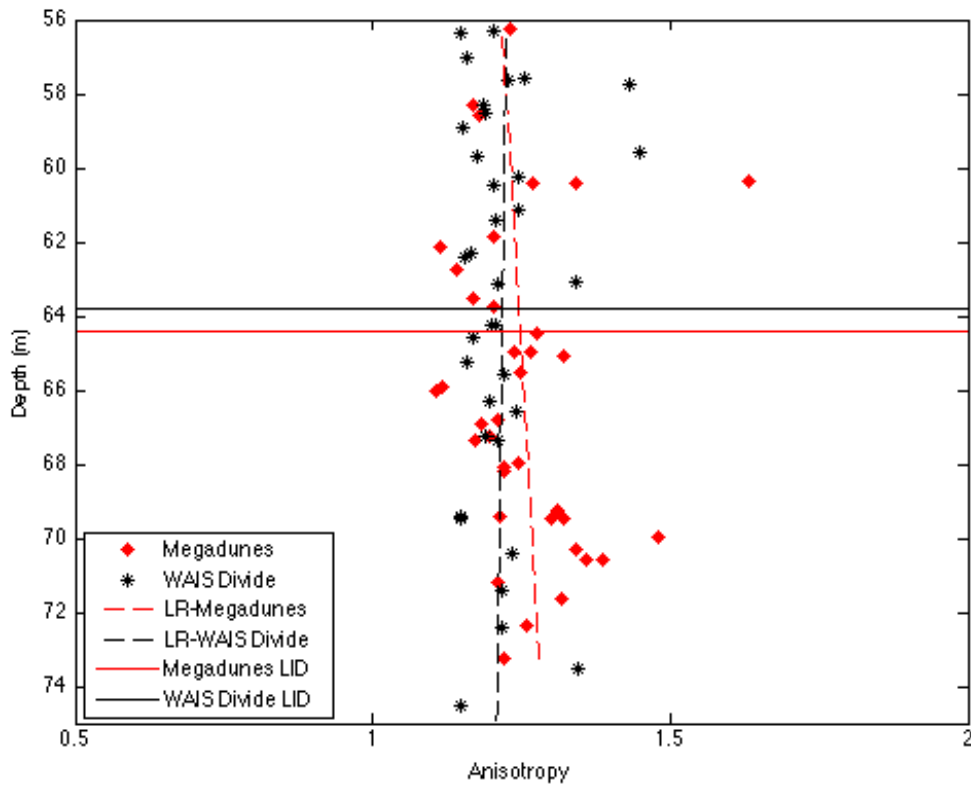


Figure 28. Anisotropy for WAIS Divide (black stars) and Megadunes (red diamonds)

Anisotropy profiles of both sites overlap and are almost completely isotropic. Using these microstructure parameters to describe pore structure, Megadunes and WAIS Divide pores are isotropic and evolving from cylindrical type shapes to spheres in deep firn. The difference occurs in tortuosity of the pore matrix, indicated by S/V, where WAIS Divide is more tortuous than Megadunes at a given depth and at a given density.

4.4.3 Porosity

Porosity of polar firn decreases with depth as firn densifies and serves as an indicator for the magnitude and type of gas transport present in the firn column. Total porosity of polar firn is the ratio of the air space to the ice matrix within a given volume. Total

porosity is a direct reflection of density in porous media, and is generally calculated directly from the measured density of bulk samples as:

$$P = (1 - \rho / \rho_{ice}) \quad (4)$$

Where P is the porosity of the sample, ρ is the density of the sample, and ρ_{ice} is the density of pure ice ($0.917 \text{ g}\cdot\text{cm}^{-3}$). While total porosity reflects the density of a sample, open porosity gives the amount of interstitial air space available for gas transport. All pores categorized as open are assumed to connect via the complex pore network to the atmosphere. In contrast, closed porosity, gives the amount of air volume completely surrounded by ice where gas transport cannot occur. All porosity measurements in this study were derived from microcomputed tomography analysis on individual firn cubes.

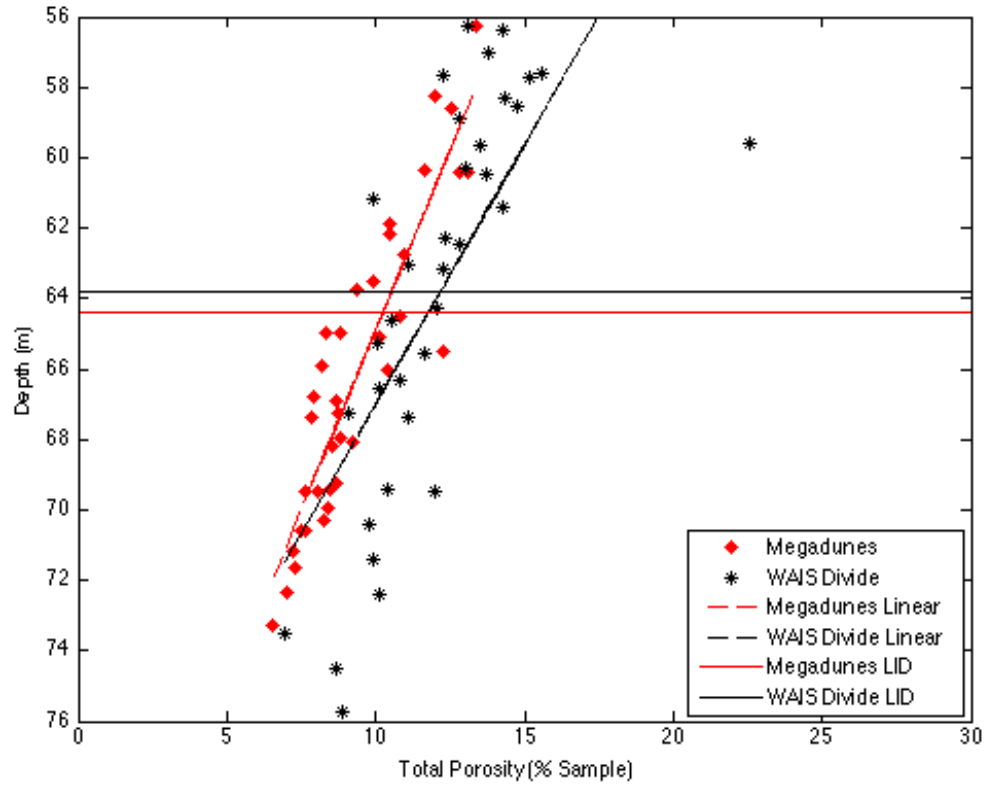


Figure 29. Total Porosity (% of sample) for Megadunes (red diamonds) and WAIS Divide (black stars)

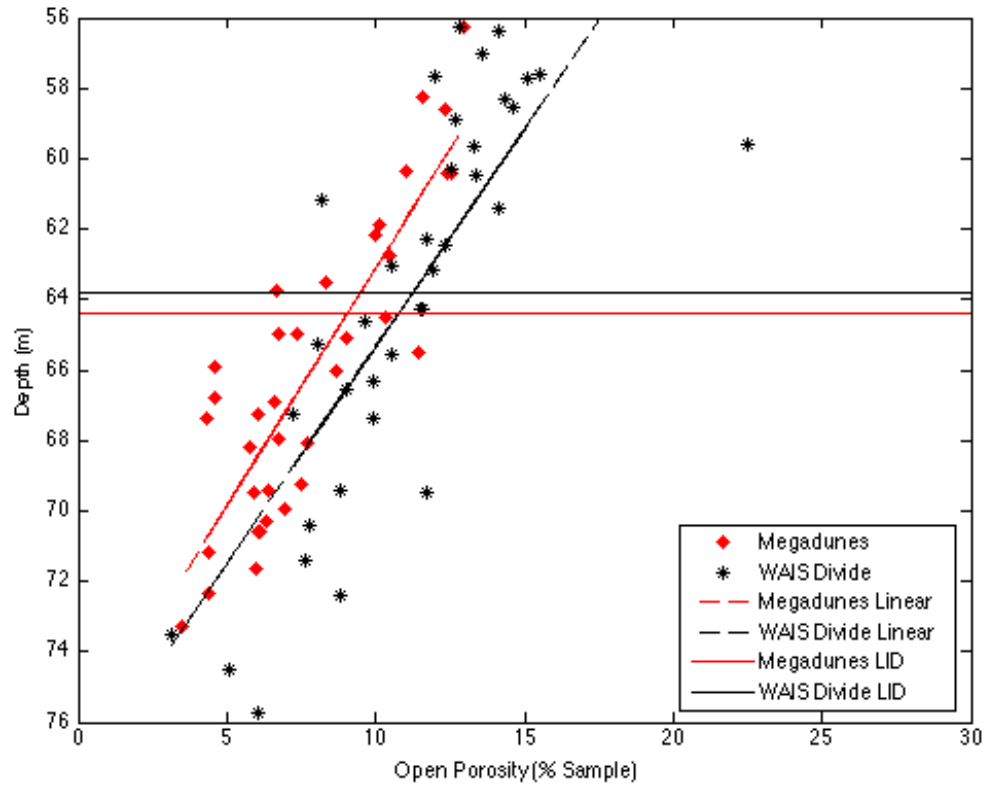


Figure 30. Open Porosity (% of sample) for Megadunes (red diamonds) and WAIS Divide (black stars)

Figures 29 and 30 show both total porosity and open porosity of Megadunes firn is consistently lower than in WAIS Divide firn at a given depth. Both total and open porosity are decreasing with depth due to the densification of firn as the pore structure becomes more segregated. Despite having lower open porosity, it is visually evident that a lower tortuosity of the pore matrix causes Megadunes firn to be more permeable than firn at WAIS Divide at a given density. A less tortuous pore structure allows for greater air flow than if the pore structure has many twists and turns.

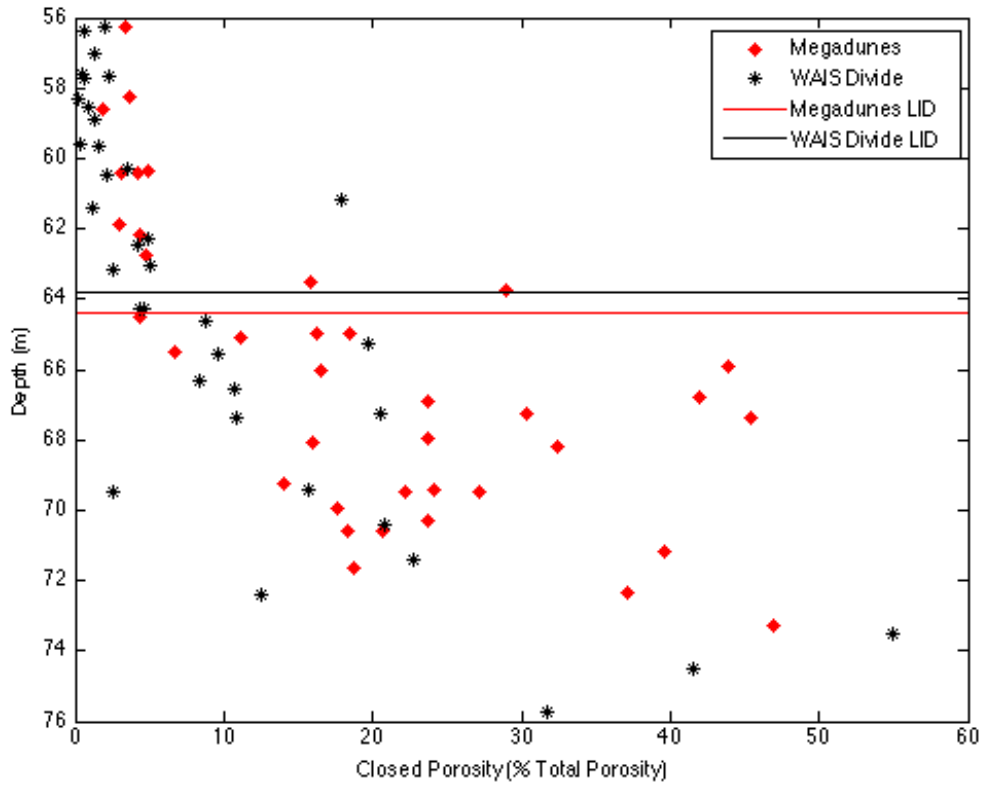


Figure 31. Closed Porosity (% of Total Porosity) for Megadunes (red diamonds) and WAIS Divide (black stars)

While total and open porosity gradually decrease with depth, closed porosity dramatically increases below the LID. Closed porosity at Megadunes and WAIS Divide is less than 8% above the LID (Figure 31). Below the LID, closed porosity increases and has greater variability. To understand the increase in closed porosity with no change seen in total porosity, the number and size of pores were examined.

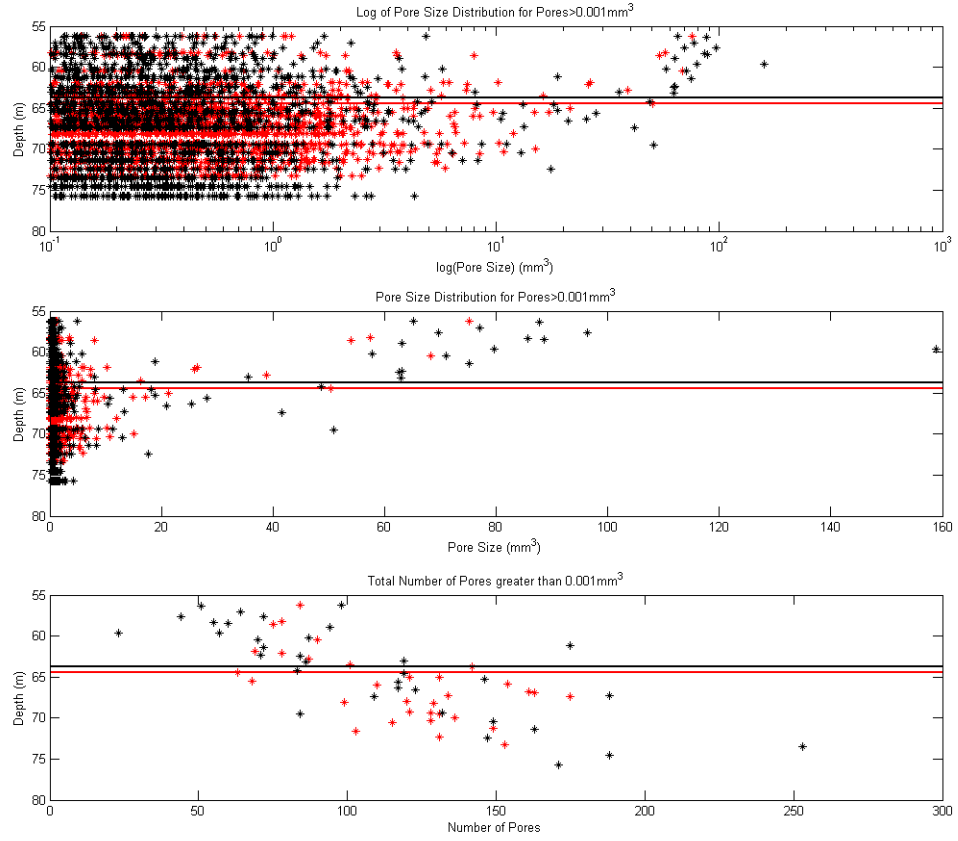


Figure 32. Profiles of log pore size (top), pore size (middle) and number of pores (bottom) of pores greater than 0.001mm^3 in deep firn, 55m to 80m, for Megadunes (red) and WAIS Divide (black).

Figure 32 shows a decrease in pore size below the LID with a large increase in the total number of pores below the LID. As pore close-off progresses, WAIS Divide has more variability in the total number of pores than Megadunes within the LIZ. This is likely due to the small scale layering of firn at high accumulation sites in comparison to firn at low accumulation sites (Landais et al., 2006, Mitchell et al., 2013, in progress). For pores less than 10 mm^3 , the pores at WAIS Divide tend to be smaller than those at Megadunes. For both sites, the abrupt increase in closed porosity at the LID corresponds with dissection of larger open pores in multiple locations to form many smaller closed or

almost closed pores. The dissection of large open pores begins at an open porosity of ~8% at Megadunes and ~11% at WAIS Divide.

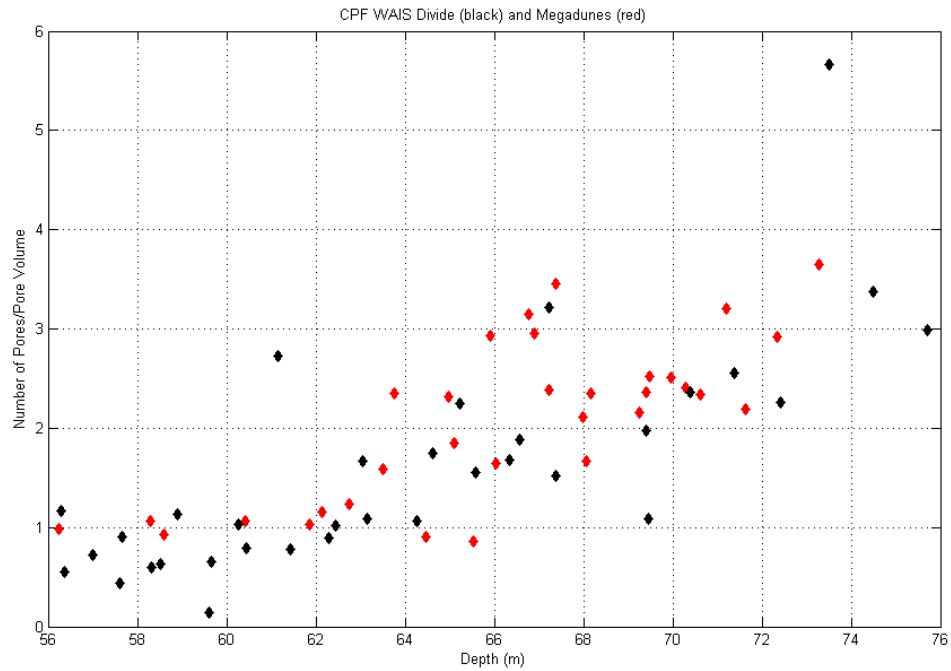


Figure 33. CPF for Megadunes (red) and WAIS Divide (black from 56-76m).

Another method used by Lomonaco et al. (2011) to observe the pore close-off process is the closed pore fraction (CPF) defined as the number of pores divided by the total pore volume of a given sample. Plotting CPF with depth for Megadunes and WAIS Divide, Figure 7, shows a steady CPF of ~1, slightly lower for WAIS Divide, until a depth of 63m. Below 63m, the CPF increases with depth at a constant slope through the LIZ. While the magnitude of CPF is slightly lower in the present study, the same trend in the rate of CPF increase, was observed through the LIZ at Summit by Lomonaco et al. (2011). The increase in CPF in the LIZ of polar firn is the result of large open pores that are abruptly dissected by the ice matrix initiating the LIZ. As firn is a layered material,

variability in CPF is due to microstructural differences between fine grained and coarse grained firn.

5 Discussion

5.1 Impact of Megadunes on Δ age

5.1.1 Shallow LID due to Antidunes Presence

The lock-in depth of present day firn columns can be determined in-situ through firn air measurements or after the core has been drilled, in the laboratory through permeability measurements. Due to the three dimensional nature of the firn the lock-in depth is defined as the depth at which multiple sequential samples are impermeable assuming horizontal homogeneity at depth in the firn column.

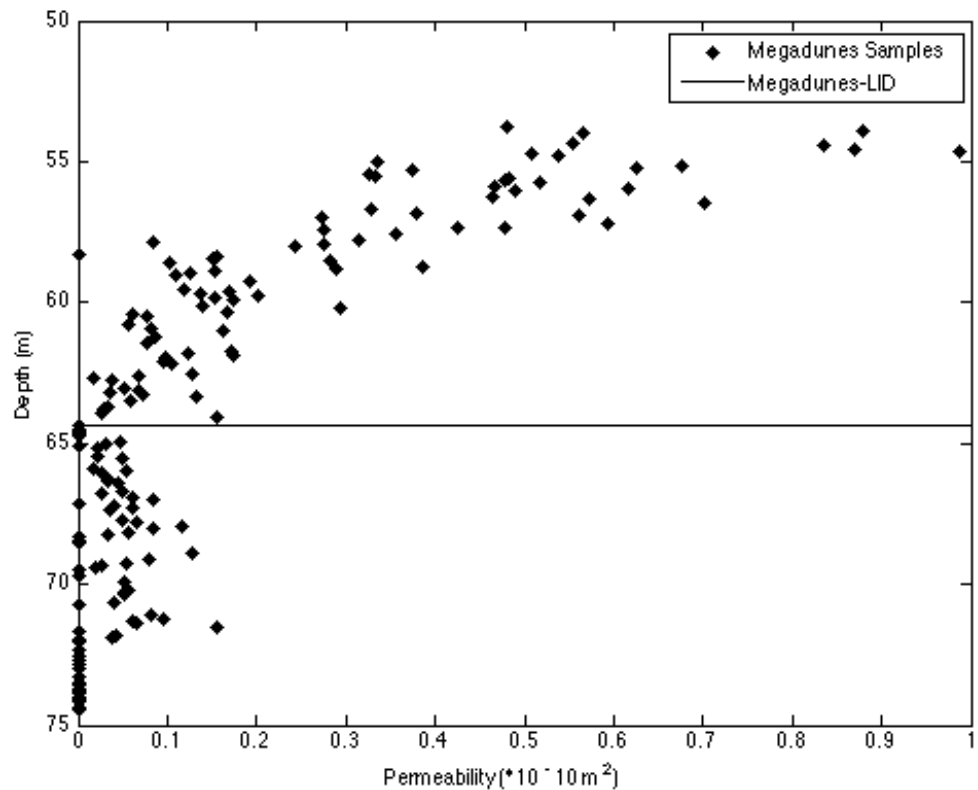


Figure 34. Permeability profile of Megadunes from 53m to 75m. The LID is at 64.4m.

Figure 34 shows the permeability profile surrounding the lock-in depth at Megadunes. The firn has permeabilities ranging from $0.3 \times 10^{-10} \text{ m}^2$ to $1.0 \times 10^{-10} \text{ m}^2$ at 55m

depth. A lone impermeable sample occurs at a depth of 58.3m and is not considered the LID due to the 3D nature of polar firn. The LID occurs at 64.4m where multiple sequential samples are impermeable. Below the LID, also known as the lock-in zone, alternating permeable and impermeable samples continue until all samples have zero permeability signifying total pore close-off or the close-off depth. Within the lock-in zone no permeability is greater than $0.2 \times 10^{-10} \text{ m}^2$. In agreement with permeability measurements, firn air measurements done by Severinghaus et al. (2010) determine the LID to be 64.5m based on sharp inflection points in the CO_2 and CH_4 data and a deviation in the slope of $\delta^{15}\text{N}$ concentrations with depth signaling the end of the diffusive zone.

The LID of sites with similar climate conditions to Megadunes (-49°C , $<4\text{cm weq yr}^{-1}$) such as Vostok and Dome C are much deeper. Table 6 shows the accumulation rate, average surface temperature, measured LID (LID) and modeled close-off depth ($\text{COD}_{\text{model}}$) (Landais et al., 2006) after models of Arnaud et al., (2000) and Barnola et al., (1991).

Site	Accumulation Rate (ice eq yr^{-1})	Average Surface Temperature ($^\circ\text{C}$)	LID (m)	$\text{COD}_{\text{model}}$ (Arnaud et al., 2000) (m)	$\text{COD}_{\text{model}}$ (Barnola et al., 1991) (m)
Vostok	2.4	-55.5	100	100	100
Dome C	2.7	-54.5	98	100	100

Table 6. Pore close-off modeled results for Vostok, Antarctica and Dome C.

Comparison with sites of similar climatic conditions shows that the LID observed through firn air measurements and permeability measurements at Megadunes is significantly shallower (64.4m) than the measured LID at both Vostok and Dome C (100m and 98m respectively). The firn densification models also predict a deeper LID of 100m for both sites (Landais et al., 2006).

To understand the 35m discrepancy between the expected LID at a site like Megadunes and the observed LID at Megadunes the physical properties of the firn are examined. Surface observations made at antidune locations (Frezzotti et al., 2002 and Courville et al., 2007) show accumulation sites, with $3-4\text{cm weq yr}^{-1}$, on the windward side of the dune have a microstructure consisting of small closely packed fine grains. In contrast, the hiatus or ablation sites, with 0cm weq yr^{-1} , on the leeward faces and troughs, have a microstructure consisting of large faceted grains (Courville et al., 2007). Ground penetrating radar, figure 35, taken of the site by Ted Scambos shows alternating diagonal light and dark bands where past dune faces have been buried as the antidunes migrate upwind. The radar line was taken 300m off-profile of the borehole giving approximate dune face locations.

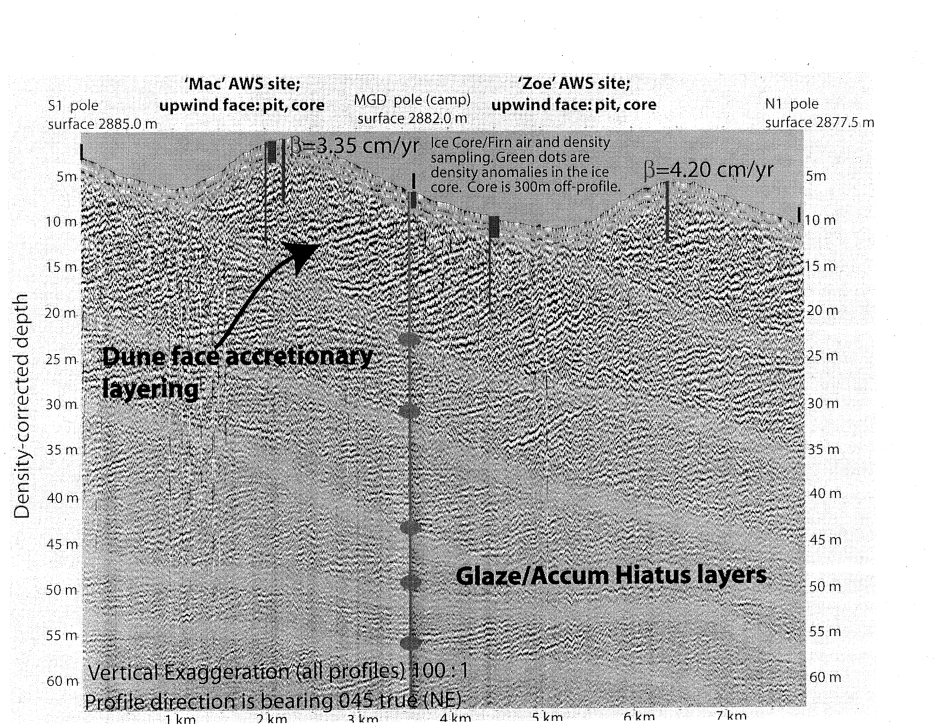


Figure 35. Radar image of dune propagation through firn column down to 65m depth from the Megadunes site (Ted Scambos).

Another distinction between the accumulation sites and hiatus sites are the large number of wind crusts present at the accumulation site in comparison to only a few wind crusts very close to the surface present at transition and hiatus sites which disappear with depth (Courville, PhD Thesis).

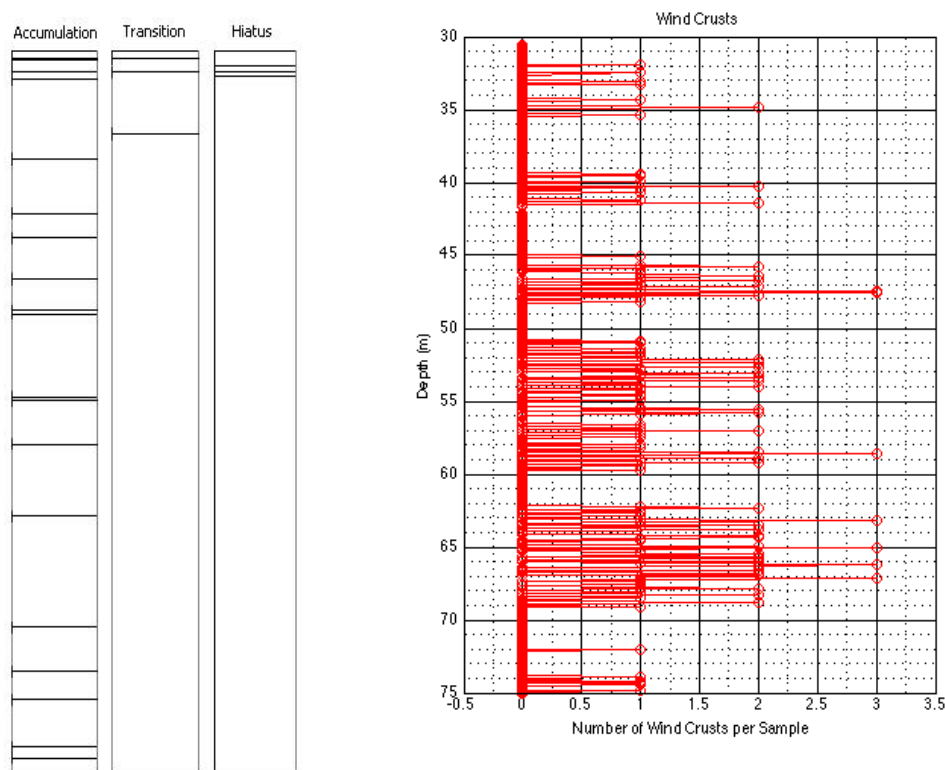


Figure 36. Wind crust frequency in surface snow pits, top 120cm (Courville, PhD Thesis) and in the firn column between 30m and 75m.

Figure 36 shows the relationship between wind crusts and surface site characteristics. The large number of wind crusts present at only the accumulation site allows us to use wind crusts as a proxy down through the firn column for when past accumulation sites dissect the borehole in conjunction with visual stratigraphy. As the dunes are buried and compressed their frequency with depth increases. The rate at which

the dunes migrated upwind and their spatial variability in the past could also affect their frequency in the column. Combining the radar image, wind crust frequency, and visual stratigraphy, past accumulation sites pass through the firn column at the drill location at 20m, 35m, 40m, 47m, 53m, 58m, and 64m. Below 64m, the distinction between dunes becomes harder to observe due to an increase in frequency.

Permeability gives an indication of pore structure and responds to the enduring signature of past hiatus and accumulation sites.

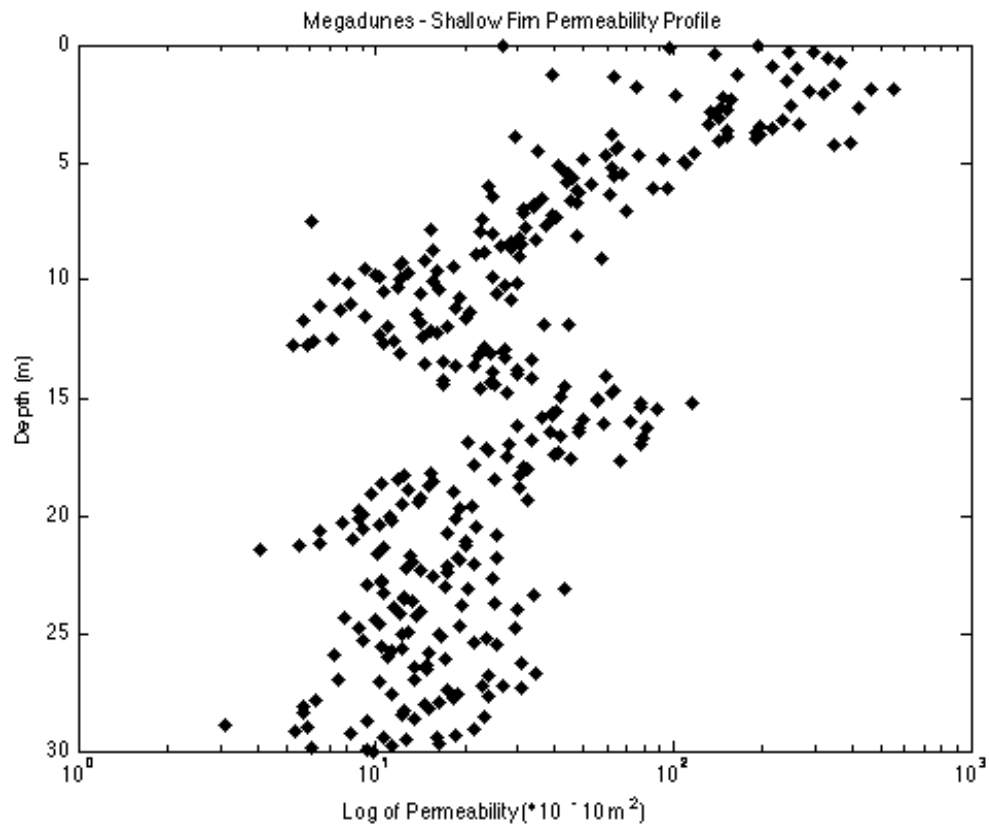


Figure 37. Top 30m of Megadunes log of permeability profile with depth (Courville, PhD Thesis).

In figure 37, in the top 30m of the firn column, permeability measurements increase due to coarse grains (past hiatus site) around 15m and 24m while decreasing due to fine grains (accumulation site) around 20m and again near 30m as the accumulation site at

35m is approached. At depth, decreases in permeability occur at depths coincident with past accumulation sites. Looking back at figure 34, the locally impermeable sample at 58.3m occurs in the middle of an accumulation site characterized by small grains and lower overall porosity. Multiple impermeable samples starting at 64.4m indicating the LID also occur in a past accumulation site. Below the LID the increased frequency of the dunes causes the variability in permeability until total pore close-off.

Without the presence of the antidunes at Megadunes, and the subsequent propagation of distinct accumulation sites (fine grained) down through the firn column, the LID would not have occurred at 64.4m. The LID would have likely been much deeper, approximately 100m on par with the LID observed and modeled for Vostok and Dome C (Landais et al., 2006). The alternate locations of accumulation and ablation at the surface of Megadunes creates meter scale layering of the firn column much different than the firn found at any other present day site and it is therefore unsurprising that using the average accumulation rate and temperature at Megadunes to model firn densification would not capture the correct behavior of the firn and would overestimate the LID.

5.1.2 Antidunes and the data-model mismatch

A shallow LID and the propensity for deep convection due to antidunes decreases the length of the diffusive column causing lower concentrations of $\delta^{15}\text{N}$ to become trapped into bubbles. $\delta^{15}\text{N}$ concentrations at the LID of Megadunes relates to a diffusive column height of 41m (Severinghaus et al., 2010) yet the modeled LID of 100m, of sites similar to Megadunes, would add an additional 35m to the diffusive column height and an increase in gravitational fractionation would be expected. Knowing that antidunes alter the LID and subsequently lowers $\delta^{15}\text{N}$ concentrations points to flaws in the firn

densification models for the large data-model mismatch. Recently Parrenin et al. (2013) used tie points between Dome C and Dronning Maud Land over the last glacial transition to determine a Δ age that showed good agreement with those estimated from $\delta^{15}\text{N}$ measurements at Dome C.

We postulate that the overestimation of LID from firn densification models during glacial-interglacial transitions and glacial periods at very low accumulation sites could be due to a shallow LID the direct result of inhomogeneous accumulation and antidunes. Antidunes decrease the amount of $\delta^{15}\text{N}$ gravitational fractionation from two mechanisms, deep convection; due to high surface permeability and macro cracks at ablation sites, and a shallow LID; due to premature pore close-off of firn originating as a past accumulation site. Firn densification models have no way to capture the unsteady-state behavior of an antidunes site, specifically the pronounced differences between zero accumulation or ablation and 2cm weq yr^{-1} , a fingerprint of antidunes. Courville et al. (2007) gave three main indications that may be present in deep ice cores to identify an antidunes presence at the site: 1) A hiatus band will show up as a thick, uniform layer without any annual cycles present, 2) the ice will show more evidence of post depositional processing, and 3) there would likely be altered isotopic and chemical species concentrations.

An overestimation in LID at a low accumulation site leads to a large overestimate in Δ age. An overestimation of 35m in LID at an accumulation rate of 2cm weq yr^{-1} accounts for up to 2,000 years in the age of the ice. If antidunes were present during glacial periods, for sites such as Vostok, Dome Fuji, and Dome C, the overestimation of LID seen in firn densification models would be expected because the steady-state assumption and calibration properties do not apply under antidunes conditions. A

shallow LID and the propensity for deep convection due to antidunes decreases the length of the diffusive column leading to low values of $\delta^{15}\text{N}$ trapped within the core which is typical of glacial time periods. The shallow LID reduces the necessity for excessively deep convective zones of up to 40m to resolve the data-model mismatch during glacial and transition periods. Relying on firn densification models for past LID at very low accumulation sites outside of present day climate conditions creates a Δage too large, during climatic conditions typical of antidunes formation. A decrease in Δage due to the presence of antidunes could decrease much of the discrepancy and controversy that currently exists in the synchronicity of atmospheric CO₂ and temperature seen during glacial-interglacial transitions.

5.2 Layering in Polar Firn

Layering at WAIS Divide occurs much differently than at Megadunes due to a significantly higher accumulation rate of 22 cm yr⁻¹ ice equivalent and an absence of antidunes. At WAIS Divide distinct summer and winter layers are formed within which individual storm events can be distinguished. Annual layers at the depth of the lock-in zone are approximately 0.25m thick (Mitchell et al., 2013) which one would expect to lead to high permeability variability on the half meter scale due to multiple seasons present and their variability in density and pore structure. The relative difference in permeability is defined as:

$$\Delta k_{\text{rel}} = [(k_{\text{max}} - k_{\text{min}})/k_{\text{avg}}] * 100 \quad (10)$$

Where k_{max} and k_{min} are the maximum and minimum permeabilities present in a half-meter range and k_{avg} is the average permeability of all samples within half a meter. The relative difference rather than the absolute difference is used in order to compare between

various depths at a single site and between two sites. This calculation was done on both Megadunes and WAIS Divide firn from 55m through the lock-in zone to pore close-off.

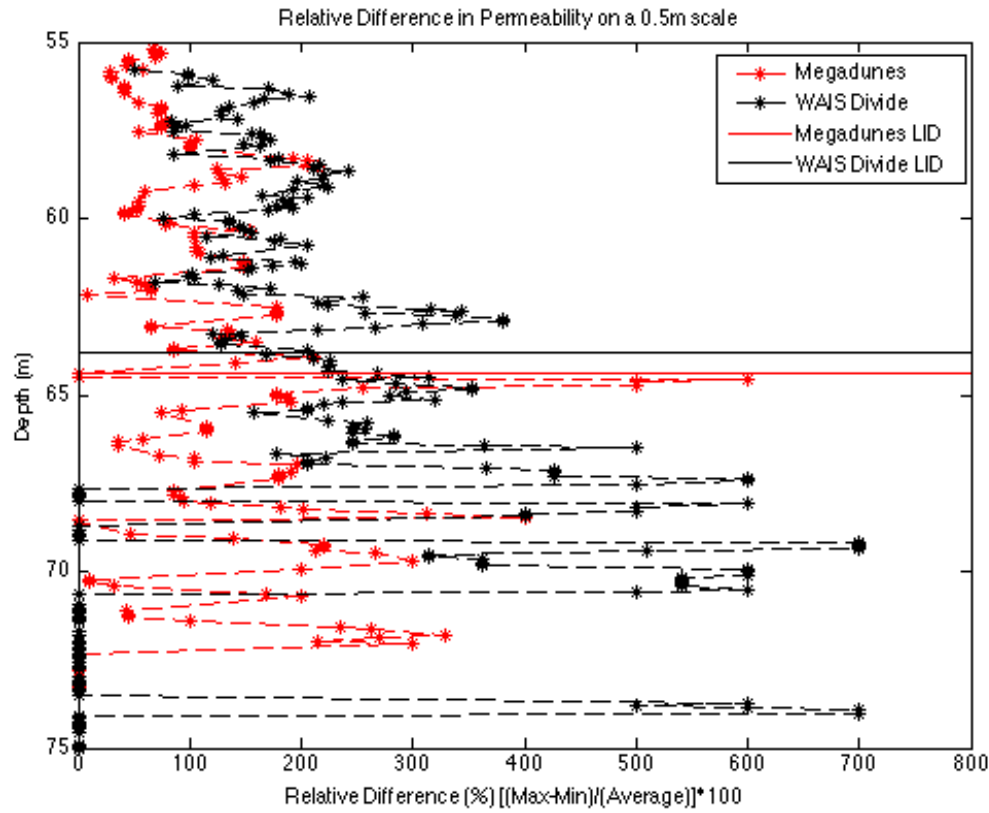


Figure 38. Relative Difference in Permeability on a half-meter scale from 55m through pore close-off. Megadunes (red) and WAIS Divide (black).

Figure 38 shows WAIS Divide as having consistently higher permeability variability until the start of the lock-in zone agreeing with the hypothesis that inter-annual variations due to initial surface deposition influences the gas transport in deep firn. Once the lock-in zone is reached with many samples having zero permeability, the relative difference in permeability sky-rockets due impermeable firn layers and no longer serves as an indicator of inter-annual microstructural firn properties. The centimeter scale

microstructure layering causes a large depth and density range of impermeable samples creating a larger lock-in zone at WAIS Divide than at Megadunes.

Looking at permeability variability as an indication of layering between Megadunes and WAIS Divide indicates that high accumulation sites retain more centimeter scale layering. This small scale layering is the result of surface deposition and short residency time on the surface of the ice sheet in comparison to low accumulation sites, where snow crystals sit on the surface for much longer causing the firn to coarsen and homogenize on the centimeter scale (Albert et al, 2004, Rick and Albert, 2004). The presence of antidunes at the Megadunes location is unique for a low accumulation site, and leads to meter scale layering affects within the firn column as the antidunes migrate upwind and are subsequently buried. As the dunes are buried and compressed the affects of their layering happen over smaller and smaller depth ranges. If dunes are not present at low accumulation sites, the time a portion of firn sits at the surface and within the firn column, up to ten times the amount of time of a high accumulation site, results in a more microstructurally homogenous firn column showing little to no lock-in zone, a feature noted by Landais et al. (2006). In contrast, high accumulation rates, such as that seen at WAIS Divide, increase microstructural variability on the centimeter scale causing high and low permeability layers to exist within close proximity to each other. Often these layers correspond to winter and summer layers but can be the result of individual storm events as well. In conjunction with the lock-in zone lengths observed in this study, measurements of lock-in zone length during firn air campaigns across Antarctica and Greenland show longer lock-in zones at high accumulation sites and shorter to no lock-in

zone at low accumulation sites (Landais et al, 2006, Battle et al, 1996, Etheridge et al, 1996, Schwander et al 1993, Battle et al, 2011, Severinghaus et al, 2010).

5.3 Impact of physical properties on pore close-off

5.3.1 Macroscopic Properties: Density and Permeability

Density and permeability measurements made between 30-36 m and 55-80 m at Megadunes and WAIS Divide are displayed in Figure 39. For both sites, the 30-36 m depths are many meters above the lock-in zone, and the lock-in zone falls within the 55-80 m depths. It can be seen from the overall profiles that in the 30-36 m depths above the lock-in zone, the Megadunes site is much more permeable than the WAIS Divide site. Their density profiles at this depth range are similar. In addition, it is evident that even for a given density in the 30-36 m depth range, Megadunes firn is more permeable than WAIS Divide firn, above the lock-in zone.

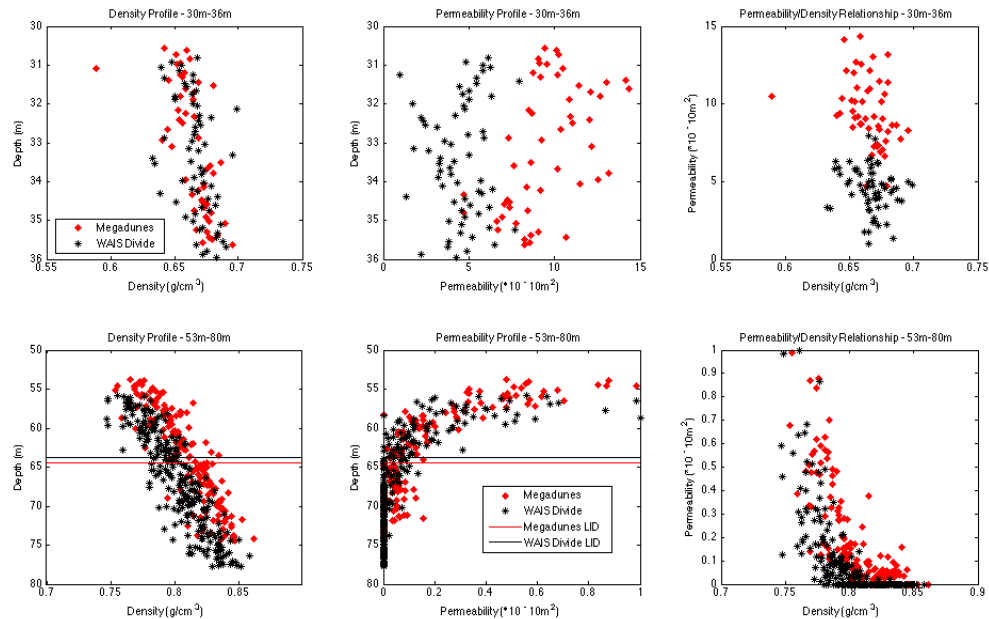


Figure 39. Density 30m-36m (top right), permeability 30m-36m (top middle), density/permeability relationship 30m-36m (top left), density 55m-80m (bottom right),

permeability 55m-80m (bottom middle), density/permeability relationship 55m-80m (bottom left) for WAIS Divide (black) and Megadunes (red).

The relationships are different within the lock-in zone. For depths between 55-80 m just above and within the lock in zone, it can be seen from figure 39 that Megadunes firn is more dense than WAIS Divide but the permeability profiles are similar. Very near and within the lock-in zone, the relationship existing between density and permeability shows that Megadunes firn is more permeable for any given density than is the WAIS Divide firn. The LID, defined as the depth where multiple sequential samples are impermeable, is at 64.4 m at Megadunes and 63.8 m at WAIS Divide indicated by a red and black line respectively.

5.3.2 Application to densification models and LIZ characteristics

Pore close-off is traditionally defined in layered firn as the process in which individual layers of firn become impermeable and proceeds until all layers are impermeable or closed-off. In the current literature on pore close-off, density controls the depth at which pore close-off occurs in an individual layer and dense layers are thought to close off shallower than low density layers (Martinerie et al., 1992). Combining density driven pore close-off and noting the density cross-over observed in polar firn (Horhold et al., 2011), the first firn layers in deep firn to reach pore close-off should be the high density, coarse grained layers. Our observations of close-off including microstructure and density between Megadunes and WAIS Divide suggest that microstructure, rather than density, is the main driving force for pore close-off. At depth, Megadunes firn is consistently more dense than WAIS Divide firn yet the permeability profiles above the LID and the LID for both sites are almost identical, 64.4 m and 63.8 m

respectively. To explain the lack of a direct relationship between density and permeability between Megadunes and WAIS Divide the tortuosity of the pore structure must be taken into account. Megadunes, has larger grains than WAIS Divide at a given density leading to a less tortuous pore structure causing higher permeabilities at a given density in Megadunes firn than those observed at WAIS Divide.

It should be noted that previous estimates, such as those developed by Martinerie et al. (1992) of mean pore close-off density are almost directly at the peak of a Gaussian type density distribution for all impermeable layers within the lock-in zone at each site, figure 40. Megadunes, a cold site with an average temperature of -49°C, has a predicted mean pore close-off density of $0.830 \text{ g}\cdot\text{cm}^{-3}$ higher than $0.821 \text{ g}\cdot\text{cm}^{-3}$ at WAIS Divide, a warmer site with an average temperature of -31°C . The density range of the distribution and length of the LIZ, are dependent upon the microstructure variability between firn layers and agree with Landais et al. (2006) who postulated that low accumulation sites will have smaller lock-in zones from an homogenous firn column and lack of annual layering.

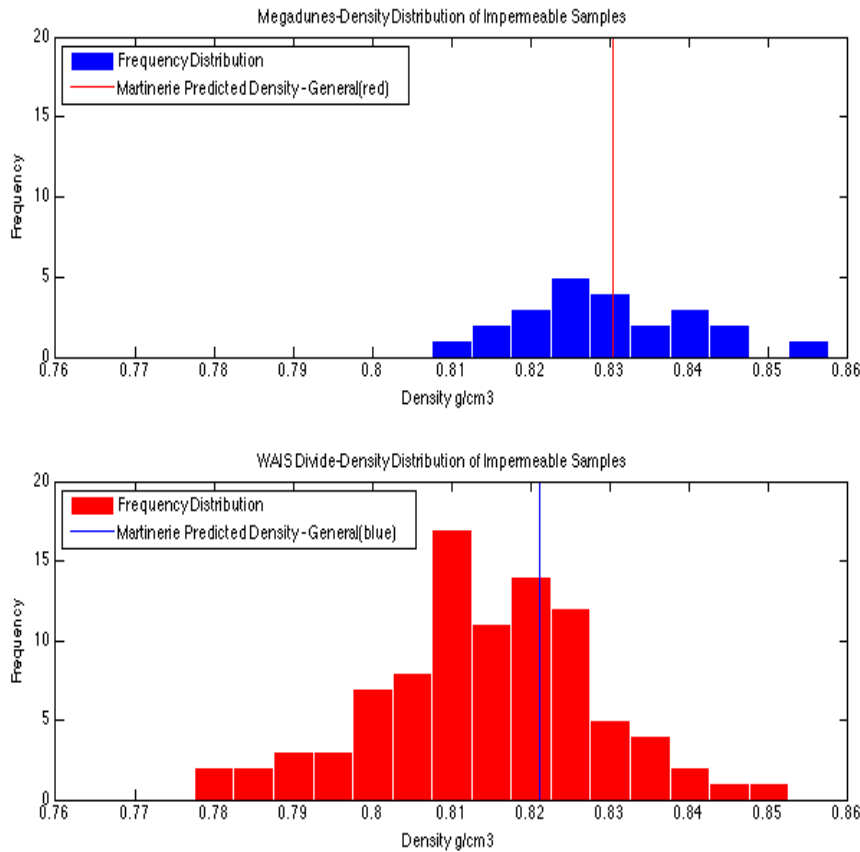


Figure 40. Density distribution of impermeable firn samples from the LID to the end of the LIZ where all samples are impermeable at Megadunes (top) and WAIS Divide (bottom). Martinerie predictions of pore close-off density are shown as vertical lines.

While comparison between two sites of significantly different local climates reveals that microstructure plays a significant role in dictating permeability and pore close-off, identifying the same trend at an individual site would further strengthen our hypothesis and constrain the impact of temperature verse accumulation rate on the process. Both Megadunes and WAIS Divide were individually analyzed by identifying fine grained and coarse grained layers within the firn column and observing their relationship with both density and permeability.

As commonly seen in polar sites, WAIS Divide firn exhibits a density cross-over in which initially high density layers consisting of fine grained firn are less dense than

corresponding initially low density layers consisting of coarse grained firn.

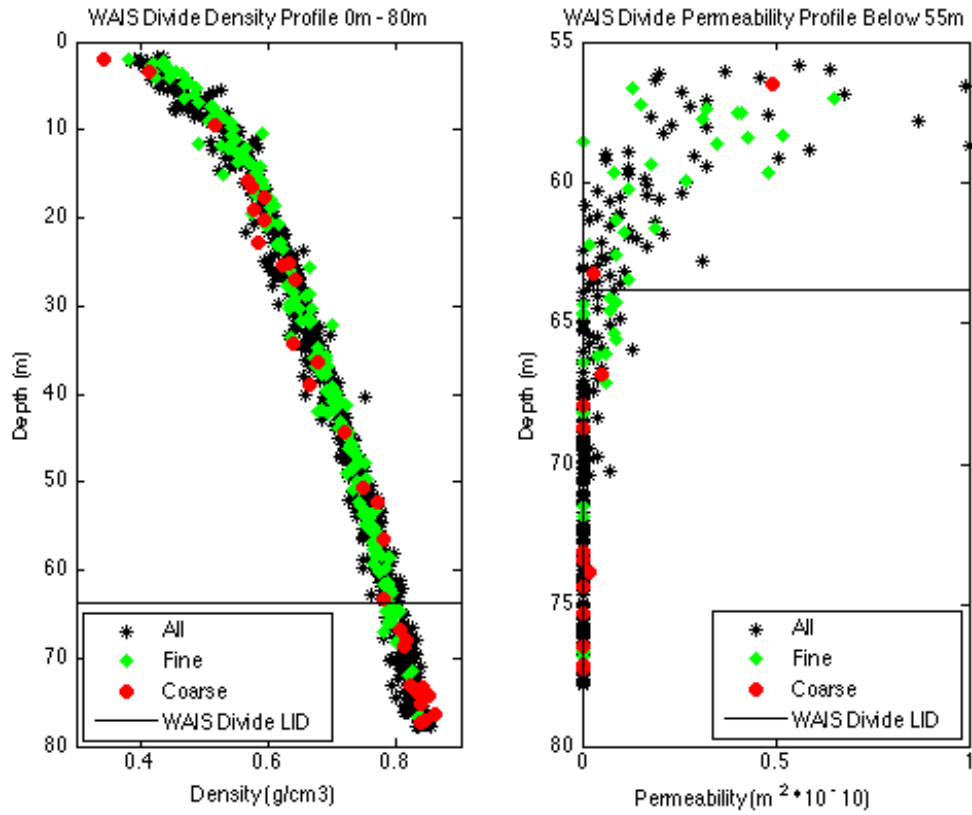


Figure 41. Density cross-over of fine and coarse gain firn at WAIS Divide (left) and deep firn permeability profile at WAIS Divide (right) both show fine firn (green), coarse firn (red), and intermediate firn (black).

The density cross-over in figure 41 has been noted at WAIS Divide in high resolution density measurements on firn core WDC06A done by Kreutz et al. (2011) with a minima in density variability occurring around 30 m. In the right plot of figure 9, fine grained layers become impermeable shallower than coarse grained layers and a coarse grained layer is the last permeable layer of the LIZ. Therefore, despite having a lower density at depth, fine grained firn reaches pore close-off first at WAIS Divide. This implies that accumulation and near surface metamorphism resulting in either fine grained or coarse grained layers, independent of temperature, remain as identifiable features of

the layers as they propagate down the column, leading to shallower pore close-off in fine grain layers at WAIS Divide.

In contrast, Megadunes does not exhibit a density cross-over and initially dense fine grained firn at surface accumulation sites on the upwind dune face remains more dense than coarse grained firn from surface hiatus sites on the leeward dune face through pore close-off. The fine grained, dense firn originating from a past accumulation site at Megadunes becomes the first impermeable layers initiating the start of the LIZ. The ability of fine grained firn to become impermeable before coarse grained firn in this study at both WAIS Divide and Megadunes, as well as in previous studies (Freitag et al., 2004) regardless of whether or not it was the predominately dense layer at depth emphasizes the importance of grain size and pore structure when predicting gas transport and pore close-off in polar firn. A recent study by Horhold et al. (2011) correlated an increase in accumulation rate to an increase in density variability in deep firn leading to longer LIZs. While we agree that density variability due to layering does indeed increase for high accumulation sites, the density cross-over seen in most polar firn sites leads to an inverse relationship of density and microstructure in deep firn where fine grained layers are less dense than coarse grained layers. Because they are both based on the layering, microstructure will have high layer-to-layer variability in places where layering also makes the density variable. The microstructure variability between fine grained and coarse grained layers, likely of the same magnitude of the density variability observed by Horhold et al. (2011), controls the length of the LIZ. For polar sites, fine grained layers should reach pore close-off at shallower depths than coarse grained layers. To capture this behavior, firn densification models should include two pore close-off densities, one

corresponding to the finest grained layers that will predict the LID and one corresponding to the coarsest grained layers that will predict the COD. In this way, the LID, COD, and LIZ length can be accurately estimated based on the accumulation rate of a site and the resulting microstructure variability. While Megadunes is unique due to the presence of buried antidunes, we believe that low accumulation sites should exhibit less microstructure variability in deep firn following trends of density variability developed by Horhold et al. (2011) for low accumulation sites. Separate close-off densities for fine grained and coarse grained firn should be utilized to define the LIZ in firn densification models at both high and low accumulation sites based on our observations of microstructure dependent close-off.

For a physical description of why fine grain firn reaches pore close-off first, we hypothesize that the grain size of the ice and neck size of the pore structure in firn leads to a threshold in open porosity corresponding to pore close-off in a single layer of firn. Freitag et al. (2004) found that coarse grained layers densify at a quicker rate than fine grained layers but the pore size of both layers decreased at the same rate. Therefore in conjunction with our findings, whichever layer has smaller pores at the surface (the fine grained layer) should close-off first. Rick and Albert (2004) and Courville et al. (2007) both found that buried layers retain evidence of their character when they were in the near-surface firn. The larger grains at Megadunes and subsequent larger pore necks enables the firn at Megadunes to reach a higher density and lower open porosity of ~8% before the open pore space is quickly dissected into many smaller closed pores. At WAIS Divide, the open porosity threshold occurs higher at ~11% open porosity, due to the smaller ice grains and smaller necks in the pore structure. For a given accumulation

rate, fine grained firn will have the highest open porosity at pore close-off, coarse grained firn layers will have the lowest open porosity at pore close-off and intermediate grain size layers should have open porosity thresholds for close-off in between the two extremes. Extrapolating this relationship across a variety of accumulation rates, high accumulation rates typically lead to smaller grains and should have high open porosity (>10%), low density at pore close-off while low accumulation sites with larger grains should have low open porosity (<10%), high density at pore close-off.

5.3.3 Application to Firn Air Models

Increasing the understanding of how microstructure affects diffusivity in deep firn through the LIZ should decrease the necessity for inverse modeling based on present day firn air measurements within firn gas transport models. Initial diffusivity profiles within polar firn are typically modeled off the Schwander et al. (1988) parameterization of firn tortuosity as a function of porosity, despite recognition by Fabre et al. (2000) who found that tortuosity profiles are site to site dependent. A recent attempt to model permeability and diffusivity as a function of open porosity, was done by Freitag et al., (2002) on 3D reconstructed firn cubes. The permeability constant k was fit to open porosity with the following power law:

$$k=10^{-7.7} \cdot n_{op}^{3.4} \quad (11)$$

where n_{op} is the open porosity of the sample (Freitag et al., 2002). The power law fit allowed for permeable firn below 0.12 open porosity the threshold for permeable firn in previous studies done by Fabre et al. (2000) and Schwander et al. (1988).

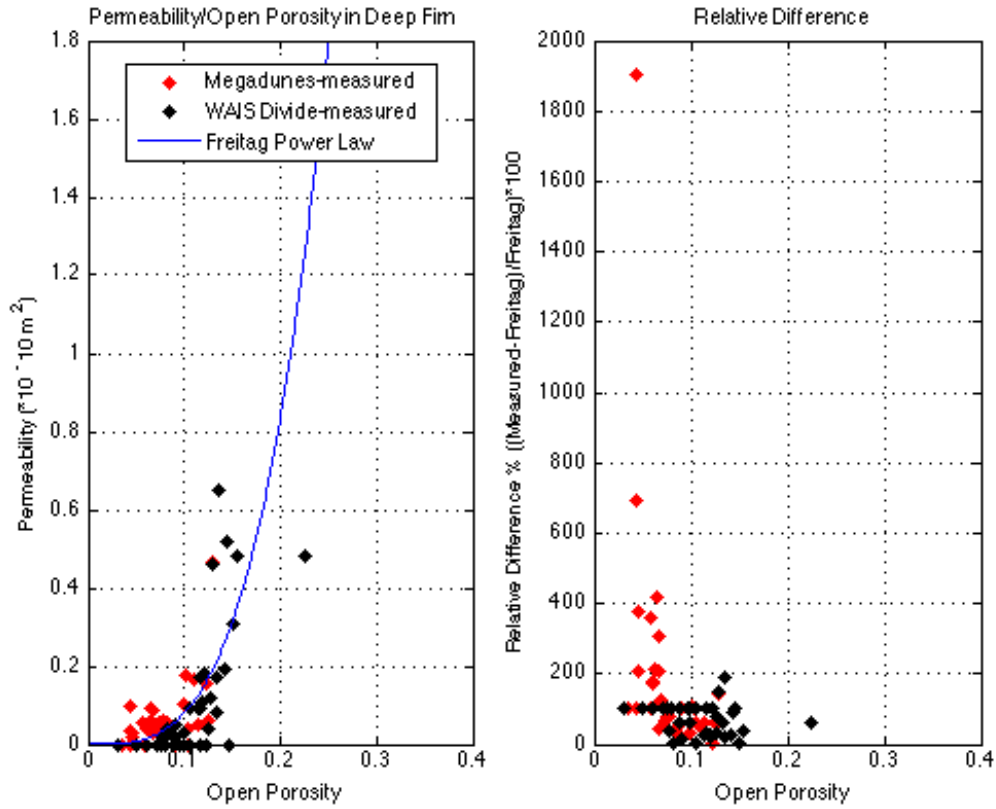


Figure 42. Measured and predicted (blue line, Freitag et al., 2002) permeability values (left) and relative error (right) for Megadunes (red) and WAIS Divide (black).

Plotting permeability data for Megadunes and WAIS Divide in figure 42 shows high scatter around the power law fit from measured permeability for both sites, though the general curve of the power law can be seen. The power law function fails most at low open porosity values (5-10%) at Megadunes where the firn is 200-700% more permeable than predicted with the power law function. The large error at Megadunes is likely due to the large difference in local climate at Megadunes in comparison to the climate of Greenland where the firn in the Freitag et al. (2002) study originated. The dependence of pore structure, on grain size and accumulation rate, influences gas transport in the diffusive column along with controlling pore close-off. The low accumulation rate, large grain size, and larger less tortuous pore structure at Megadunes enables the firn to be

much more permeable than predicted by Freitag et al. (2002). As WAIS Divide has a local climate much similar to Greenland, the error between modeled and measured permeability is not as large.

In deep firn it has been shown that diffusivity and permeability are linearly related (Adolph et al., 2013) and thus the connection between permeability and grain size/pore structure can be extrapolated to diffusivity. Firn air models that use density profiles derived from firn densification models to determine the open porosity which is then used to calculate the effective diffusivity profile of a specific gas (Buizert et al., 2012) will fall short of capturing the true nature of gas transport in deep firn. A given open porosity at a high accumulation site will lead to lower observed gas diffusivity than the diffusivity observed at a low accumulation site. The microstructure must be accounted for to improve physics based models of diffusivity in polar firn. The dependence of grain size on accumulation rate and near surface residence time observed by Albert et al. (2004), Rick and Albert (2004), Courville et al. (2007), and Fujita et al. (2009) along with an increase in gas transport due to an increase in grain size shown in this study could be used to create site specific effective open porosity profiles. An effective open porosity profile derived from local climate parameters, specifically accumulation rate, which captures gas transport dependence on pore structure, should improve forward firn air modeling. If the physics of forward firn air modeling can be accurately captured through climate parameters it should reduce the need for inverse modeling and enhance the reliability of forward modeling of past firn columns where inverse modeling is not plausible.

5.3.4 Summary of local climate impacts on pore close-off and gas transport

Microstructure is the main driving force for pore close-off in which fine grained firn is seen to reach pore-close off at shallower depths than coarse grained firn regardless of density. These results should be incorporated into firn densification models by the inclusion of two pore close-off densities; one for the finest grained layers which would give the LID and one for coarsest grained layers corresponding to the COD. Because they are both based on the layering, microstructure in highly-layered firn will have high variability in places where layering also makes the density variable. Thus the microstructure will have high variability in the deep firn of high accumulation sites. In relation to pore close-off, a threshold is seen in open porosity, a result of accumulation rate and near surface grain size propagating down the firn column into deep firn. At porosities lower than the threshold (>10% for high accumulation sites and <10% for low accumulation sites), closed porosity increases rapidly, total number of pores increases at a greater rate, and the size of pores dramatically decreases (many small pores opposed to a few large open pores). Parameterizing pore close-off with both grain size and density, along with the layered nature of firn in firn densification models would improve their ability to accurately predict the LID and LIZ length.

Firn air models should include an effective open porosity that accounts for differences in pore structure between high and low accumulation rate sites. An effective open porosity that reflects the pore structure of the site, not simply how much pore space is present, that correctly captures permeability in deep firn may provide better understanding of gas transport in the LIZ. An increase in the physical understanding of pore close-off in polar firn and its dependence upon local climate will enable more

accurate modeling under firn conditions with no present day analogue constraining the gas age/ice age difference.

6 Conclusion

Understanding the influence of anthropogenic inputs on the Earth's climate system first requires a base understanding of climatic fluctuations and abrupt climate change of the past. Of specific importance is the phasing between temperature and atmospheric carbon dioxide during glacial-interglacial transitions. Accurate prescriptions of gas age and ice age at a given depth within an ice core are necessary because the air, the source of CO₂ concentrations is always younger than the surrounding ice, the source of temperature. The ice age/gas age difference, Δ age, is due to the process of air entrapment in the upper 100 meters of an ice sheet. The top 50-100m of an ice sheet consists of polar firn, a porous media spanning the densification ranges between snow and glacial ice. Polar firn essentially acts as filter smoothing atmospheric signals as air rapidly diffuses to the base of the firn column on a decadal scale (Sowers et al., 1992, Schwander et al., 1997). The magnitude of Δ age is largely driven by the accumulation rate at a given site and thus understanding how accumulation rate and other local climate signals influence the microstructure, gas transport, and pore close-off within polar firn is of vital importance. The density, permeability and microstructure of two firn cores from different local climates, WAIS Divide and Megadunes, were examined. The microstructure of the firn, specifically the grain size and pore structure, was determined to have a significant impact on permeability and pore close-off that is not demonstrable directly through density variability.

Antidunes (Megadunes) and their inhomogeneous nature of accumulation rate deposition, create a unique firn column with meter scale layering through the propagation down through the firn column of microstructural characteristics developed at the surface.

The alteration between past zero accumulation or ablating surface sites and accumulation sites provides a natural experiment independent of temperature in which past accumulation sites close-off earlier than firn densification models predict based on the average accumulation rate and temperature of the site. The presence of antidunes during glacial and glacial-interglacial transitions at very low accumulation sites in East Antarctica would decrease Δ age adding additional constraints on the relationship between atmospheric CO₂ and temperature.

The physical characteristics of deep firn near the lock-in zone in deep firn at WAIS Divide and Megadunes gave a link between the gas transport properties and microstructural variability within polar firn. The open pore structure plays a more important role than density in predicting gas transport properties, through the porous firn matrix. For both WAIS Divide and Megadunes, fine grained layers experience close-off shallower in the firn column than do coarse grained layers, regardless of which grain sized layer is the more dense layer at depth. Pore close-off occurs at an open porosity that is accumulation rate dependent. Low accumulation sites, with coarse grains, close-off at lower open porosities (<10%) than the open porosity (>10%) of high accumulation sites with finer grains.

At a given density, Megadunes firn pore structure was less complex and tortuous and therefore resulted in higher permeabilities than WAIS Divide firn, characterized by smaller grains and a more complex pore structure. The depth and length of the lock-in zone is primarily dependent upon accumulation rate and microstructural variability due to differences in grain size and pore structure, rather than the density variability of the layers. The pore close-off process should start with fine grained layers and progress with

depth toward coarse grained layers. The greater the variability between fine and coarse grain layers, the larger the depth interval this would happen over. Typically high accumulation sites show more layering at depth than low accumulation sites leading to long lock-in zones under high accumulation conditions (Landais et al., 2006, Horhold et al., 2011). Characterization of the lock-in zone based on firn microstructure and density at depth should improve firn densification models.

A proposed way to incorporate the findings of this thesis into firn densification models is to determine the lock-in depth based on the finest grained firn reaching a site and grain size specific close-off density and to determine the close-off depth based on the coarsest grained firn reaching a second site and grain size specific close-off density. Therefore two critical close-off densities should be established at each site based on the local climate and extent of microstructure variability at depth.

Implications for forward, physics based firn air modeling derived from this work include establishing an effective open porosity profile from the densification profile that is accumulation rate dependent. As low accumulation leads to a longer residence time in the near surface, coarser grains will be developed enhancing gas transport at a given density in deep firn. The opposite holds true for high accumulation sites, whose grains remain small leading to a complex, tortuous pore structure that dampens gas transport. Improving forward based model should reduce the need for inverse modeling and increase the confidence of firn air modeling when firn air measurements are not plausible. Relating pore close-off to microstructure at both WAIS Divide and Megadunes has enabled an accumulation rate, grain size dependent understanding of the lock-in zone. Application of these findings on the pore close-off process in polar firn could reduce the

data-model mismatch during glacial periods and glacial-interglacial transitions if antidunes were present, improve modeling of the lock-in zone through firn densification models, and reduce the need for inverse firn air modeling.

7. Future Work

Future work should be divided into two main focus areas:

1. Antidunes, specifically chemistry and impurity analysis on the dunes as they propagate down the firn column and become glacial ice. While antidunes have the potential to decrease Δ age in the past, establishing a signature for antidunes that is maintained in deep ice cores is necessary for the application of a shallow LID.
2. Examination of sites from a wide variety of local climates in order to further develop the dependence of gas transport and pore close-off on pore structure, grain size, and climatic condition.

References

1. Schwander, J., T. Sowers, J.M. Barnola, T. Blunier, A. Fuchs, and B. Malaizé (1997), Age scale of the air in the summit ice: Implication for glacial-interglacial temperature change, *J. Geophys. Res.*, 102(D16), 19,483-19,492.
2. Sowers T., M. Bender (1992), ^{15}N of N_2 in air trapped in polar ice: a tracer gas transport in the firn and possible constraint on ice age-gas age differences. *Journal of Geophysical Research*, 97: 15683-15697.
3. Bender M., T. Sowers, E. Brook (1997), Gasses in ice cores. *Proceedings of the National Academy of Science*, 94: 8343-8349.
4. Severinghaus, J. P., Grachev, A., and Battle, M. (2001). Thermal fractionation of air in polar firn by seasonal temperature gradients. *Geochem. Geophys. Geosy.*, 2.
5. Kaspers, K. A., van de Wal, R. S. W., van den Broeke, M. R., Schwander, J., van Lipzig, N. P. M., and Brenninkmeijer, C. A. M. (2004). Model calculations of the age of firn air across the Antarctic continent. *Atmos. Chem. Phys.*, 4(5):1365-1380.
6. Landais, A., Barnola, J. M., Kawamura, K., Caillon, N., Delmotte, M., Van Ommen, T., Dreyfus, G., Jouzel, J., Masson-Delmotte, V., Minster, B., Freitag, J., Leuenberger, M., Schwander, J., Huber, C., Etheridge, D., and Morgan, V. (2006). Firn-air delta N-15 in modern polar sites and glacial-interglacial ice: a model-data mismatch during glacial periods in antarctica? *Quaternary Sci. Rev.*, 25(1-2):49-62.
7. Hörhold, M. W., Kipfstuhl, S., Wilhelms, F., Freitag, J., and Frenzel, A. (2011), The densification of layered polar firn, *J. Geophys. Res.-Earth Surf.*, 116.
8. Herron, M.M. and C.C. Langway (1980), Firn densification: an empirical model, *J. Glaciol.*, 25(93), 373-385.
9. Martinerie, P., D. Raynaud, D.M. Etheridge, J.M. Barnola, and D. Mazaudier (1992), Physical and climatic parameters which influence the air content in polar ice, *Earth Planet. Sci. Lett.*, 112, 1-13.
10. Goujon, C., Barnola, J. M., and Ritz, C. (2003). Modeling the densification of polar firn including heat diffusion: Application to close-off characteristics and gas isotopic fractionation for Antarctica and greenland sites. *J. Geophys. Res.-Atm.*, 108(D24):18.
11. Mitchell et al., 2013, in progress
12. Barnola, J. M., Pimienta, P., Raynaud, D., and Korotkevich, Y. S. (1991). Co2-climate relationship as deduced from the vostok ice core - a reexamination based on new measurements and on a reevaluation of the air dating. *Tellus B*, 43(2):83-90. ISI Document Delivery No.: FG714 Times Cited: 119 Cited Reference Count: 0.
13. Arnaud, L., Barnola, J.-M., and Duval, P. (2000) Physical modeling of the densification of snow/firn and ice in the upper part of polar ice sheets, in: *Physics of Ice Core Records*, edited by: Hondoh, T., Hokkaido University Press, Sapporo, Japan, 285-305.
14. Severinghaus, J. P., Albert, M. R., Courville, Z. R., Fahnestock, M. A., Kawamura, K., Montzka, S. A., Muhle, J., Scambos, T. A., Shields, E., Shuman, C. A., Suwa, M., Tans, P., and Weiss, R. F. (2010). Deep air convection in the firn at a zero-accumulation site, central antarctica. *Earth Planet Sc. Lett.*, 293(3-4):359-367.
15. Colebeck, S.C. (1993), The vapor diffusion coefficient for snow, *Water Resour. Res.*, 29(1), 109-115.
16. Albert, M.R., C. Shuman, Z. Courville, R. Bauer, M. Fahnestock, and T. Scambos (2004), Extreme firn metamorphism: impact of decades of vapor transport on near-surface firn at a low-accumulation glazed site on the East Antarctic Plateau,

- Ann. Glaciol.*, 39, 73–78.
17. Alley, R.B. (1988). Concerning the deposition and diagenesis of strata in polar firn. *Journal of Glaciology* 34, 283-290.
 18. Swinkels F.B., M.F. Ashby,(1980), A second report on sintering diagrams. *Metallurgica*, 29: 259-281.
 19. Chen S. (2008), *Characterizing Dry Snow Metamorphism*. Proposal (PhD). Dartmouth College.
 20. Freitag, J., F. Wilhelms, and S. Kipfstuhl (2004), Microstructure-dependent densification of polar firn derived from X-ray microtomography, *J. Glaciol.* 50(169) 243-250.
 21. Hörhold, M. W., Laepple, T., Freitag, J., Bigler, M., Fischer, H., & Kipfstuhl, S. (2012). On the impact of impurities on the densification of polar firn. *Earth and Planetary Science Letters*, 325, 93-99.
 22. Courville, Z., Hörlhold, M., Hopkins, M., and Albert, M. (2010). Lattice-boltzmann modeling of the air permeability of polar firn. *J. Geophys. Res.*, 115(F4):F04032.
 23. Freitag, J., U. Dobrindt, and J. Kipfstuhl (2002), A new method for predicting transport properties of polar firn with respect to gases on the pore-space scale, *Ann. Glaciol.* 35, 538-544.
 24. Albert, M.R., E. Shultz, and F. Perron (2000), Snow and firn permeability measurements at Siple Dome, Antarctica, *Ann. Glaciol.*, 31, 353–356.
 25. Rick, U., and M.R. Albert (2004), Firn microstructure impacts on air permeability, *ERDC-CRREL Technical Report TR-96*, U.S. Army Corps of Engin., Cold Regions Res. and Engin. Lab., Hanover, NH, 79 pp.
 26. Courville, Zoe, et al. (2007), Impacts of an accumulation hiatus on the physical properties of firn at a low-accumulation polar site. *Journal of Geophysical Research*, Vol 112 F02030
 27. Adolph et al., in progress
 28. Fabre, A., J.-M. Barnola, L. Arnaud and J. Chappellez (2000), Determination of gas diffusivity in polar firn: comparison between experimental measurements and inverse modeling, *Geophys. Res. Lett.*, 27(4) 557-560.
 29. Dullien, F. A. L. (1975). Single phase flow through porous media and pore structure. *The Chemical Engineering Journal*, 10(1):1–34.
 30. Schwander, J., B. Stauffer, and A. Sigg (1988), Air mixing in firn and the age of the air at pore close-off, *Ann. Glaciol.*, 10, 141-145.
 31. Adolph, A., & Albert, M. R. (2013). An improved technique to measure firn diffusivity. *International Journal of Heat and Mass Transfer*, 61, 598-604.
 32. Craig H., Y. Horibe, T. Sowers (1988). Gravitation separation of gasses and isotopes in polar ice caps. *Science*, 242: 1675-1678.
 33. Weiler, K., Schwander, J., Leuenberger, M., Blunier, T., Mulvaney, R., Anderson, P. S., Salmon, R., and Sturges, W. T. (2009). Seasonal Variations of Isotope Ratios and CO₂ Concentrations in Firn Air, volume 68, pages 247–272. Institute of Low Temperature Science, Hokkaido University, Sapporo.
 34. Fain X., C.P. Ferrari, A. Dommergue, M. Albert, M. Battle, L. Arnaud, J.M. Barnola, W. Cairns, C. Barbante, C. Boutron (2008), Mercury in the snow and firn at Summit Station, central Greenland and implications for the study of past atmospheric mercury levels. *Atmospheric Chemistry and Physics*, 8: 3441-3457.
 35. Clark, I. D., Henderson, L., Chappellaz, J., Fisher, D., Koerner, R., Worthy, D. E. J., Kotzer, T., Norman, A.-L., and Barnola, J.-M. (2007). CO₂ isotopes as tracers of firn air diffusion and age in an arctic ice cap with summer melting, devon island, canada. *J. Geophys. Res.*, 112.
 36. Buizert, C., Martinerie, P., Petrenko, V. V., Severinghaus, J. P., Trudinger, C. M., Witrant, E., Rosen, J. L., Orsi, A. J., Rubino, M., Etheridge, D. M., Steele, L. P., Hogan, C., Laube, J. C., Sturges, W. T., Levchenko, V. A., Smith, A. M., Levin,

- I., Conway, T. J., Dlugokencky, E. J., Lang, P. M., Kawamura, K., Jenk, T. M., White, J. W. C., Sowers, T., Schwander, J., and Blunier, T. (2011). Gas transport in firn: multiple-tracer characterisation and model intercomparison for neem, northern greenland. *Atmos. Chem. Phys. Discuss.*, 11:15975–16021.
37. Kawamura, K., Severinghaus, J. P., Ishidoya, S., Sugawara, S., Hashida, G., Motoyama, H., Fujii, Y., Aoki, S., and Nakazawa, T. (2006). Convective mixing of air in firn at four polar sites. *Earth Planet Sc. Lett.*, 244(3-4):672–682.
38. Schwander J., J.M. Barnola, C. Andrie, M. Leuenberger, A. Ludin, D. Raynaud, B. Stauffer (1993), The age of air in firn and ice at Summit, Greenland. *Journal of Geophysical Research*, 98: 2831-2838.
39. Witrant, É., Martinerie, P., Hogan, C., Laube, J. C., Kawamura, K., Capron, E., Montzka, S. A., Dlugokencky, E. J., Etheridge, D., Blunier, T., and Sturges, W. T. (2011). A new multi-gas constrained model of trace gas non-homogeneous transport in firn: evaluation and behavior at eleven polar sites. *Atmos. Chem. Phys. Discuss.*, 11(8):23029–23080.
40. Etheridge, D. M., Steele, L. P., Langenfelds, R. L., Francey, R. J., Barnola, J. M., and Morgan, V. I. (1996). Natural and anthropogenic changes in atmospheric co₂ over the last 1000 years from air in antarctic ice and firn. *J. Geophys. Res.*, 101(D2):4115–4128.
41. Trudinger, C. M. (2001). The carbon cycle over the last 1000 years inferred from inversion of ice core data. PhD thesis, Monash University, Australia.
42. Buizert C. (2013) Studies of Firn Air. In: Elias S.A. (ed.) *The Encyclopedia of Quaternary Science*, vol. 2, pp. 361-372.
43. Buizert, C., Martinerie, P., Petrenko, V. V., Severinghaus, J. P., Trudinger, C. M., Witrant, E., Rosen, J. L., Orsi, A. J., Rubino, M., Etheridge, D. M., Steele, L. P., Hogan, C., Laube, J. C., Sturges, W. T., Levchenko, V. A., Smith, A. M., Levin, I., Conway, T. J., Dlugokencky, E. J., Lang, P. M., Kawamura, K., Jenk, T. M., White, J. W. C., Sowers, T., Schwander, J., and Blunier, T. (2011). Gas transport in firn: multiple-tracer characterisation and model intercomparison for neem, northern greenland. *Atmos. Chem. Phys. Discuss.*, 11:15975–16021.
44. Trudinger, C.M., I.G. Enting, D.M. Etheridge, R.J. Francey, V.A. Levchenko, L.P. Steele, D. Raynaud, and L. Arnaud (1997), Modeling air movement and bubble trapping in firn, *J. Geophys. Res.*, 102(D6), 6747-6763.
45. Braūnlich, M., Aballanin, O., Marik, T., Jockel, P., Brenninkmeijer, C. A. M., Chappellaz, J., Barnola, J. M., Mulvaney, R., and Sturges, W. T. (2001). Changes in the global atmospheric methane budget over the last decades inferred from c-13 and d isotopic analysis of antarctic firn air. *J. Geophys. Res.-Atm.*, 106(D17):20465–20481.
46. Aydin, M., Verhulst, K. R., Saltzman, E. S., Battle, M. O., Montzka, S. A., Blake, D. R., Tang, Q., and Prather, M. J. (2011). Recent decreases in fossil-fuel emissions of ethane and methane derived from firn air. *Nature*, 476(7359):198–201.
47. Assonov, S. S., Brenninkmeijer, C. A. M., Jockel, P. J., Mulvaney, R., Bernard, S., and Chappellaz, J. (2007). Evidence for a co increase in the sh during the 20th century based on firn air samples from berkner island, antarctica. *Atmos. Chem. Phys.*, 7:295–308.
48. Loulergue, L., Parrenin, F., Blunier, T., Barnola, J. M., Spahni, R., Schilt, A., Raisbeck, G., and Chappellaz, J. (2007). New constraints on the gas age-ice age difference along the epica ice cores, 0-50 kyr. *Climate of the Past*, 3(3):527–540. ISI Document Delivery No.: 215CJ Times Cited: 3 Cited Reference Count: 68 Loulergue, L. Parrenin, F. Blunier, T. Barnola, J.-M. Spahni, R. Schilt, A. Raisbeck, G. Chappellaz, J.
49. Capron, E., Landais, A., Buiron, D., Cauquoin, A., Chappellaz, J., Debret, M., Jouzel, J., Leuenberger, M., Martinerie, P., Masson-Delmotte, V., Mulvaney, R.,

- Parrenin, F., and Prie, F. (2012), Glacial-interglacial dynamics of Antarctic firn: comparison between simulations and ice core air- δ 15N measurements, *Clim. Past Discuss.*, accepted.
50. Dreyfus, G. B., Jouzel, J., Bender, M. L., Landais, A., Masson-Delmotte, V., and Leuenberger, M. (2010). Firn processes and δ 15n: potential for a gas-phase climate proxy. *Quaternary Sci. Rev.*, 29(1-2):28–42.
51. Parrenin, Frédéric, Valérie Masson-Delmotte, Peter Köhler, Dominique Raynaud, Didier Paillard, J. Schwander, C. Barbante, A. Landais, Anna Wegner, and J. Jouzel. (2013) "Synchronous change of atmospheric CO₂ and Antarctic temperature during the last deglacial warming." *Science* 339, no. 6123: 1060–1063.
52. Alley, R.B., J.F. Bolzan and I.M. Whillans. (1982). Polar firn densification and grain growth. *Annals of Glaciology* 3, 7-11.
53. Taina, I.A., Heck, R.J., Elliot, T.R. (2008), Application of X-ray computed tomography to soil science: a literature review. *Canadian Journal of Soil Science*, 88, 1–20.
54. Coleou C, Lesaffre B, Brzoska JB, Ludwig W, Boller E.: Three-dimensional snow images by X-ray microtomography. *Ann. Glaciol.*, 32: 75-81, 2001.
55. Schneebeli M, Sokratov SA. (2004), Tomography of temperature gradient metamorphism of snow and associated changes in heat conductivity. *Hydrological Processes* 18, 3655-3665.
56. Lomonaco, R., Albert, M., & Baker, I. (2011), Microstructural evolution of fine-grained layers through the firn column at Summit, Greenland. *Journal of Glaciology*, 57(204), 755-762.
57. Fujita, S., Okuyama, J., Hori, A., and Hondoh, T. (2009). Metamorphism of stratified firn at dome fuji, antarctica: A mechanism for local insolation modulation of gas transport conditions during bubble close off. *J. Geophys. Res.*, 114.
58. Horhold, M. W., Albert, M. R., & Freitag, J. (2009). The impact of accumulation rate on anisotropy and air permeability of polar firn at a high-accumulation site. *Journal of Glaciology*, 55(192), 625-630.
59. Frezzotti, M., S. Gandolfi, and S. Urbini (2002), Snow megadunes in Antarctica: Sedimentary structure and genesis, *J. Geophys. Res.*, 107(D18), 4344, doi:10.1029/2001JD000673.
60. Fahnestock, M.A., T.A. Scambos, C.A. Shuman, R.J. Arthern, D.P. Winebrenner, and R. Kwok (2000), Snow megadune fields on the Eastern Antarctic Plateau: Extreme atmosphere–ice interaction, *Geophys. Res. Lett.*, 27(22), 3719–3722.
61. Banta, J., McConnell, J., Frey, M., Bales, R., and Taylor, K. (2008), Spatial and temporal variability in snow accumulation at the West Antarctic Ice Sheet Divide over recent centuries, *J. Geophys. Res.*, 113, D23102, doi:10.1029/2008JD010235.
62. Garboczi, E. J. (1990). Permeability, diffusivity, and microstructural parameters: a critical review. *Cement and concrete research*, 20(4), 591-601.
63. Landis, E. N., & Keane, D. T. (2010), X-ray microtomography. *Materials Characterization*, 61(12), 1305-1316.
64. Ketcham, R. A., & Carlson, W. D. (2001), Acquisition, optimization and interpretation of X-ray computed tomographic imagery: applications to the geosciences. *Computers & Geosciences*, 27(4), 381-400.
65. Hildebrand, T. and P. Ru^üegsegger. (1997). Quantification of bone microarchitecture with the structure model index. *Comput. Meth. Biomed. Eng.*, 1(1), 15–23.
66. Kaempfer, T. U., & Schneebeli, M. (2007). Observation of isothermal metamorphism of new snow and interpretation as a sintering process. *Journal of Geophysical Research: Atmospheres (1984–2012)*, 112(D24).

67. Hori, A., et al. (1999), A detailed density profile of the Dome Fuji (Antarctica) shallow ice core by X-ray transmission method, *Ann. Glaciol.*, **29**, 211–214, doi:10.3189/172756499781821157.
68. Gerland, S., Oerter, H., Kipfstuhl, J., Wilhelms, F., Miller, H., & Miners, W. D. (1999). Density log of a 181 m long ice core from Berkner Island, Antarctica. *Annals of Glaciology*, **29**(1), 215-219.
69. Kreutz, K., B. Koffman, D. Breton, and G. Hamilton. (2011). *Microparticle, Conductivity, and Density Measurements from the WAIS Divide Deep Ice Core, Antarctica*. Boulder, Colorado, USA: National Snow and Ice Data Center. <http://dx.doi.org/10.7265/N5K07264>.
70. Courville, Z.R. (2007). Gas diffusivity and air permeability of the firn from cold polar sites. (PhD thesis, Dartmouth College.).
71. Spaulding, N. E., Meese, D. A., & Baker, I. (2011). Advanced microstructural characterization of four East Antarctic firn/ice cores. *Journal of Glaciology*, **57**(205), 796-810.
72. Battle, M., M. Bender, T. Sowers, P.P. Tans, J.H. Butler, J.W. Elkins, J.T. Ellis, T. Conway, N. Zhang, P. Lang, and A.D. Clarke (1996), Atmospheric gas concentrations over the past century measured in air from firn at the South Pole, *Nature*, **383**(19), 231-235.

